MACQUARIE UNIVERSITY

Evolution of small planetary bodies: a view from carbonaceous chondrites

Jean-Antoine Gazi

Masters of Research thesis

Department of Earth and Planetary Sciences in

The Faculty of Science and Engineering,

Macquarie University, North Ryde,

Australia.

Submission date 10/10/16

MACQUARIE
University

Statement of Originality

All the work submitted in this thesis is the original work of the author except were otherwise acknowledged. No part of this thesis has previously been submitted to any other university or institution.

Signed – Jean-Antoine Gazi

10/10/16

Dated

Acknowledgments

This thesis represents the culmination of 10 months of work, in that time I have found a new appreciation for the work involved in research. It is hard to fully appreciate the time and effort that goes into making a thesis until you, yourself are in that position. Having finally come to the end of this journey, it is amazing to see how much you can learn in such a short amount of time.

I would first and foremost like to acknowledge the work of my supervisors, Sandra Piazolo and Bruce Schaefer in helping me complete this thesis and for giving me the opportunity to work with such interesting material. It isn't every day you get to work with some of the oldest material to have formed in our solar system! A special mention should be made to Sandra who tirelessly worked to give me feedback, reviews and provided regular enthusiastic discussions about my project. The dedication she shows to her craft and to her students is admirable and has definitely left a lasting impression on me.

In completing this thesis, I have had the opportunity to work with numerous people who helped me analyse my samples. I would like to firstly mention the staff that run the Geochemical Analysis Unit (GAU) here at Macquarie University. Many days were spent sitting in front of a scanning electron microscope and having you guys there made it so much more enjoyable! A special thank you to Floriana Salvemini for assisting me in using 3D visualisation software. Thanks to Manal Bebbington for getting all my samples ready when I needed them.

A shout out to my fellow MRes cohort, Victoria Elliot, Harrison Jones, Chris Corcoran and Mitch Gerdes. This year would have been boring without you guys, the constant banter kept me sane!

Lastly, a big thanks to my family for supporting through this process. I know this year would have been so much more difficult without them!

Evolution of small planetary bodies: A view from carbonaceous chondrites

Abstract

Carbonaceous chondrites offer a tangible record of the astrophysical and geological processes occurring in the early solar system. They provide insight into the formation and amalgamation of the first solids, through to the geological evolution of small planetary bodies. In this study, the macroscopic properties of chondrites are related to microscopic features of the chondritic components. The chemical and microstructural properties of chondrules from three selected, but representative CV_{oxA} chondrites are studied and a new chondrule classification scheme is presented. This new scheme is used to help identify the modification of chondrules by nebular and parent-body interactions which leads to a refined model for variable alteration of the CV parent-body. Neutron computed tomography is used to visualise and quantify the components of CV and CM type chondrites. On this basis, a simplified model for the formation of CM and CV chondrites is presented.

Chapter 1: General introduction and set-up of thesis

Introduction

Meteorites offer a tangible record of planetary formation in the protosolar nebular. The aim of studying such samples is to decipher the history and formation of their respective parent bodies (Woods, 1988; Scott, 2007). They provide a unique opportunity to understand the processes involved in planetary formation from the accretion of the earliest solids (Grossman, 1972; Fegley et al., 1985; Shu et al., 2001) to planetary differentiation, and core formation (Klein et al., 2002; Yin et al., 2002). Meteorites broadly classify into two groups; chondrites and achondrites (Prior, 1920). Achondrites represent igneous rocks that formed as melts or partial melt residues on their parent bodies (Weisberg et al., 2006). Chondrites are a group of meteorites (Suppli., Table 1.1) that exhibit a wide range of silicate and metallic minerals with an aggregate texture (Wasson & Kallemeyn, 1988). Their aggregation texture, petrography, chemical and isotopic composition give evidence of disequilibrium indicating that chondrites never experienced melting. As a result, chondrites are thought to have formed in the early solar nebula (Dodd & Schmus, 1965). The bulk chemical composition of chondrites is comparable to the non-volatile component of the photosphere and further establishes chondrites as primitive materials (Wasson & Kallemeyn, 1988). This makes studying chondrites pivotal in advancing our understanding of planetary formation.

Carbonaceous chondrites form the most diverse and rare group of chondrites, representing less than 4% of recovered meteorites (Scott, 2007). They are characterised by a relatively high abundance of carbon, oxidised elements, hydrated minerals and record the first appearance of liquid water in the solar system through the common occurrence of aqueous alteration on the chondrite parent-body (McSween, 1979). In conjunction with aqueous alteration, carbonaceous chondrites exhibit variable stages of thermal metamorphism and shock deformation, most of which occurred on the parent body (McSween, 1977; Scott et al., 1992). On this basis, carbonaceous chondrites are divided into petrographic groups (Table 1.1).

There are many unanswered questions regarding the formation of the chondritic components, the accretion of these components and the subsequent processes involved in forming the final lithology of chondrites. In particular, the understanding of chondrule formation and subsequent textural and chemical evolution in the early solar nebula and on the meteorite parent body requires further investigation.

Table 1.1 Classification of carbonaceous chondrites. Adapted from Weisberg et al. (2006)

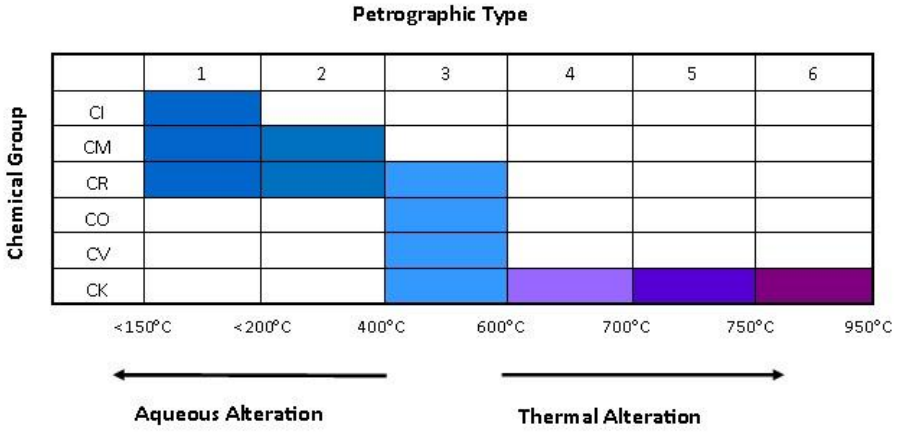

A small number of carbonaceous chondrites such as Allende, Murchison and Vigarano have been the subject of much scientific scrutiny. Our understanding of chondrite formation is derived from the alteration and accretion histories of these few chondrites. The diversity of carbonaceous chondrites gives testament to the range and complexity of processes occurring in the early solar nebula (Scott, 2007). This makes including a range of chondrites in this study pivotal in adequately investigating the question addressed in this thesis.

Aim of the study

To close the outlined gap in our knowledge, this project aims to utilize chondrules from a selected, but representative set of carbonaceous chondrites to gain an in-depth understanding of their origin and geological history spanning their formation, amalgamation, and subsequent alteration. Based on this understanding, this thesis aims to present a refined model for planetary formation and evolution. The aims of this thesis can be broken down as follows;

1) Visualise and quantify the petrography of chondrites using a novel technique i.e. neutron computed tomography.
2) Characterise chondrules in terms of geochemistry, mineralogy, and microstructures by combining state of the art techniques.
3) Establish the formation and alteration history of chondrules by subsequent gas and fluid interaction in the solar nebula and parent-body.
4) Produce a model of planetary evolution considering the chondrule diversity based on the alteration of a few ‘primary’ chondrule textures.

Chondrule characteristics, formation and significance for deciphering early solar nebula processes

General characteristics of Chondrules

Chondrites are made up of four components; chondrules, refractory inclusions, Iron (Fe)-Nickel (Ni) metal grains and fine-grained matrix (Kallemeyn & Wasson, 1981). Chondrules are typically the most abundant component of chondrites apart from a few groups which include CR, CM, CI and CK types (Suppl., Table. 1.1). They are millimetre sized silicate spherules that represent droplets of melt that cooled rapidly and subsequently crystallised primary mineral phases such as olivine, low Ca pyroxene and Fe-Ni metallic grains (Grossman et al., 1988). Chondrules are thought to have formed in the mid plane of the solar nebular during transient heating event that thermally processed amorphous pre-solar dust (Nagahara, 1981; Cuzzie et al., 2006). Radial pyroxene and barred olivine textures observed in chondrules place an upper temperature limit at 150 K – 400 K above the liquidus during these heating events (Cuzzie et al., 2006). Lead-Lead ages of chondrules vary from 46565.45+0.45 Mya (Allende CV3) to 4562.8+0.9 Mya (Hammadah al Hamara CB3), placing their formation at the earliest stages of planetary formation (Connelly et al., 2008; Krot et al., 2005). Shocks wave induced heating events represent the current favoured model of chondrule formation due to their ability to adequately reconcile the thermal history of chondrules (Krot et al., 2009). The source of shockwaves remains unclear, however collisions between planetary embryos (Hood et al., 2008), X-ray flares (Nakamoto et al., 2005) and gravitational instabilities (Boss & Durisen, 2005) in the disk are cited as possible sources.

One important constraint on chondrule formation comes from the retention of volatiles including; Sodium (Na), Potassium (K) and Sulphur (S) during melting events (Alexander et al., 2008). Hewins et al. (2005) and Nagahara et al. (2005) proposed that chondrules formed in a dense atmosphere with dust enriched 1000 times to reconcile the retention of volatiles in chondrules. These conditions provide a strong incentive to explore gas-chondrule interaction in the solar nebular. A study of chondrules in the reduced CV carbonaceous chondrite Vigarano found that the evolution of porphyritic olivine melts to porphyritic pyroxene with more silicic composition was likely driven by high SiO(g) of the surrounding nebula gas (Marrocchi & Libourel, 2013). The authors concluded that volatile enrichment from olivine to pyroxene bulk compositions resulted from a progressive reaction between partially depleted olivine bearing precursors and a volatile rich gas phase.

Chondrules are analogous to cosmic sediments forming in several source regions. On this basis, the characteristics of solar nebular source regions and how these source regions mix can be investigated.

Alteration of the carbonaceous chondrite parent-body

It is recognised that most carbonaceous chondrites recovered have been subjected to secondary processing on the chondrite parent body (McSween, 1979; Zolensky & McSween, 1988; Zolensky et al., 1993; Brearley & Jones, 1998; Krot et al., 2004). The role of fluids in the textural and chemical evolution of carbonaceous chondrites has become increasingly investigated. Mineral-fluid interaction in chondrites is described by two processes; aqueous alteration and metasomatism (Brearley & Krot, 2013). Both are fluid mediated, and result in significant change in the structure and composition of the primary phases described previously (Brearley & Krot, 2013). Aqueous alteration is a low temperature process (<80^{o}C) that has resulted in the formation of hydrated phyllosilicates, magnetite, Fe-Ni sulphides and carbonates in CM, CI and some CV chondrites (McSween, 1979; Zolensky & McSween, 1988; Zolensky et al., 1993; Brearley & Jones, 1998). In comparison, metasomatism occurred at higher temperatures (>200^{o}C) where ferrous olivine is the dominant stable phase and resulting secondary mineralisation is anhydrous (Krot et al., 2004; Zolotov et al., 2006). Secondary minerals associated with metasomatism include fayalite, nepheline, sodalite, Ca, Fe-pyroxenes, andradite, magnetite and Fe, Ni sulphides (Krot et al., 2004). Understanding the context of aqueous alteration and metasomatism on the chondrite parent is a unique challenge because there is no geological context for these samples (Brearley & Krot, 2013). What drove high and low temperature alteration on the parent-body and what the relationship between the two alteration styles is still unknown.

Formation of the chondrite lithology

Chondrites are generally interpreted to have formed by the accretion of solar nebular material with various modification of this primary texture by parent-body alteration (Krot et al., 2009). Based on the study of the Mokoia CV chondrite, Tomeoka & Ohnishi (2015) proposed that the formation of chondrite meteorites is a more complex and dynamic process. In their model, chondrules and surrounding matrix is fragmented in different regions of the parent-body. Transportation forms the final lithology with mixing and accumulation of these clasts in a fluidised state before lithification. The processes required to fragment and transport material from different source regions is poorly constrained, and further work is needed to refine this model.

Furthermore, whether this model can be applied to chondrites in general or is specific to the Mokoia lithology is yet to be investigated.

Set up of the thesis:

In this thesis, the main questions posed are addressed in form of two major chapters. Each chapter represents a publication style manuscript. A final chapter summarizes results and points to possible future directions within the research area. As the main chapters (Chapter 2 and 3) are written with the aim of been submitted to international peer-reviewed journals, some minor repetitions could not be avoided.

Chapter 1 *3D visualisation and quantification of CV and CM chondrite petrography using neutron radiography* investigates the petrography of CM and CV chondrites using neutron computed tomography. The resolution of neutron tomography has increased significantly over the last four decades and this technique is now seeing application in the quantification and visualisation of geological material. A three-dimensional analysis combined with analysis on two-dimensional sections allow new ways of sample characterization and interpretation. **Chapter 2** *Textural and chemical evolution of chondrules in CV_{oxA} chondrites: implications for nebular source regions and geological processes on small planetary bodies* details the chemistry and microstructure of chondrules to investigate the textural and chemical evolution of chondrules in the solar nebula and on the chondrite parent body. Mineral chemistry is analysed by energy dispersive spectroscopy (EDS) and Electron backscatter diffraction (EBSD) is used to analyse the microstructure of chondrules. This data is utilized to develop a new method of categorising chondrules.

Chapter 2:

Neutron computed tomography of CV and CM carbonaceous chondrites: Quantitative characterisation of their main components and its bearing on planetary formation processes

Abstract

Neutron computed tomography (NCT) is a non-destructive three-dimensional imaging technique that allows the components of geological material to be visualised and quantified. The modal abundance of the matrix material was found to correlate with abundance of altered chondrules in CV chondrites. On this basis, a model for the formation of CV and CM chondrites is presented. In this model, chondrite components from different source regions are fragmented, transported and agglomerated to form the final lithology. Sub-rounded hydrated clasts in CM samples gives direct evidence for this process. The application of neutron computed tomography to the study of chondrites is demonstrated and evaluated. For the CV3 sample (Allende) the modal abundances of CV chondrite components quantified in this study agree with results from previous studies as well as results from μx-ray based computer tomographic analysis. In comparison, NCT analysis of CM chondrites visualises reliantly the hydrated components. NCT is a useful technique for first three-dimensional characterisation of chondrite components in terms of shape, abundance and distribution.

Introduction

Planetary formation remains an enigmatic problem requiring a multi-disciplinary approach to solve its multifaceted questions. Meteorites are physical record of the earliest processes occurring in our solar system and offer unique possibilities to decipher the early history of planets (Woods, 1988; Scott, 2007). Chondrites are a group of meteorites that exhibit a wide range of silicate and metallic minerals with an aggregate texture (Scott, 2007). One major sub-group is formed by carbonaceous chondrites, which are of interest as they exhibit primitive chemical compositions like that of the photosphere (Anders & Grevesse, 1989) along with ubiquitous evidence for aqueous alteration (McSween, 1979). Carbonaceous chondrites are composed of forsterite rich, so called type I chondrules, refractory inclusions and an olivine rich matrix that can contain a range of phyllosilicates (McSween, 1977; Tomeoka & Buseck, 1985). Understanding the petrography of carbonaceous chondrites is pivotal in unravelling the processes involved in the accretion of the various chondritic components to form the final lithology of the chondrite parent body. Knowledge of the microstructures and distribution of the different chondritic components

i.e. matrix, chondrules, refractory inclusions and opaques gives important clues to how the chondrite parent body accreted.

The microstructural characteristics of carbonaceous chondrites are predominately studied using 2D petrographic techniques including optical microscopy and back-scattered electrons imaging augmented by in-situ geochemical analysis (McSween, 1979; Tomeoka & Buseck, 1985; Browning et al., 1996). While analysis of 2D sections allow the sample to be studied in detail, only a comparatively small part of the sample can be studied. The section studied may not be representative of the whole sample (Hezel et al., 2013). Sample preparation for making 2D sections is a destructive process making it difficult to study rare chondrites with little recovered material. In hydrated chondrites, great care must be taken when preparing the sample to avoid preparation induced alterations that hinder correct analysis and thus interpretations.

Neutron computed tomography (NCT) utilises the penetration and attenuation of neutrons interacting with different material to reconstruct a three-dimensional (3D) image of the object. NCT can be used as a complementary analysis technique that addresses the short comings of 2D petrographic techniques by providing true 3D characterization and direct measurement of the volume percentage of different components (Carlson, 2006; Hezel et al., 2013). In engineering, it is a well-established technique (strobl et al., 2009) however it has seen limited application in geoscience (Votonbel et al., 2005; Carlson, 2006). NCT can provide a unique visual representation of the sample which may show previously unrecognised features e.g. if altered or metal rich areas in CM and CV chondrites are discrete or interconnected. NCT allows microscopic observations to be contextualised within the macroscopic character of the chondrite sample. A further advantage of NCT is its non-destructive nature, requiring no sample preparation prior to analyses. This makes neutron imaging particularly useful when studying the 2D and 3D characteristics of rare, precious chondrites such as CI type chondrites. Furthermore, it allows quick screening of newly found meteorites to establish a first characterisation and classification.

This study represents the first application of NCT to the study of carbonaceous chondrites. 3D characteristics are visualised and quantified for chondrites including; Allende (CV), Murchison (CM), Nagoya (CM), Sutter's Mill (CM), NWA3118 (CV) and NWA4502 (CV). Of these, only Allende and Murchison have been studied in detail both petrographically in two dimensional sections and µx-ray based three-dimensional computed tomography (Hezel et al., 2013). In this study, we utilise the results to (i) advance our understanding of planetary formation processes and (ii) compare the strengths and limitations of neutron tomography in the study of chondrites.

Studied samples: current knowledge

Allende- oxidised CV3 chondrite

Allende is an oxidised meteorite and is composed of chondrules, matrix, refractory inclusions and opaque minerals. The major mineral constituents of chondrules include olivine (forsterite to Fe-rich forsterite), enstatite and Ca-rich plagioclase. Minor mineral phases reported in previous studies include; kamacite, taenite, troilite, mackinawaite, antigorite, majorite, pentlandite, magnetite and anorthite (Kornacki & Wood, 1984). The meteorite matrix is a fine-grained porous aggregate of minerals including euhedral Fa-rich olivine platelets, clinopyroxene, nepheline, sodalite, Ti-Al-pyroxene and minor feldspars (anorthite) (Kornacki & Wood, 1984). Olivine in type I chondrules have Fe-Mg zoning where Fa-rich olivine occurs along grain boundaries and fractures within olivine phenocrysts (Peck & Wood, 1987).

NWA3118- oxidised CV3 chondrite

NWA 3118 was recovered in 2013 with an original mass of ~5.9 Kg. It has a low weathering grade (Akos et al., 2014) and is composed of type I chondrules and chondrule fragments, refractory inclusions, and matrix. The matrix is composed of euhedral olivine (Fayalite rich) platelets, clinopyroxene, nepheline, sodalite, Ti-Al-pyroxene and minor anorthite. (Akos et al., 2014) observed diffuse ripple like structures in the matrix described as subparallel bands of olivine grains <10 µm enclosed by pod-like masses of µm to sub µm sized olivine pyroxenes and minor weathering products. NWA3118 also exhibits Fe-Mg zoning like that observed in Allende.

NWA4502- oxidised CV3 chondrite

NWA 4502 is composed of well-defined chondrules and chondrule fragments and refractory inclusions hosted in matrix. Olivine inside chondrules is predominately forsterite and pyroxenes are enstatite. Chondrules contain an abundance of sulphides and iron oxides. They are found as a) massive blebs of troilite (+ magnetite) inter grown with pyroxene at the edge of chondrules, b) spheroidal droplets poikilitically enclosed in pyroxenes and c) amorphous pools located in the mesostasis pockets. The meteorite matrix is a fine-grained porous aggregate of minerals dominated by µm sized Fa-rich olivine as well as µm to mm sized grains of troilite, pentlandite and magnetite. The matrix also contains rare alteration products typical of the CV3 Allende-like oxidised sub-group such as µm sized nepheline crystals and Fe-Ca rich silicates.

Murchison- CM chondrite

The Murchison meteorite is composed of matrix, chondrules and polymineralic fragments, monomineralic grains and fragments, refractory inclusions and opaque minerals (McSween, 1979). Chondrules are mainly forsterite rich with varying degrees of replacement by phyllosilicates. The matrix is predominately made up of phyllosilicates (Fe-cronstedtite and Mg-serpentine) with minor olivine, pyroxene, sulphides, calcite and magnetite (Howard et al. 2011). Based on a classification of 11 CM meteorites by Rubin et al. (2007) Murchison is one of the least altered CM chondrites with a rating of CM2.5 where CM2.0 is most and CM2.6 least hydrated.

Nagoya- CM chondrite

The Nogoya CM chondrite is a well-preserved fall with ~4kg of material recovered. Most of the primary silicates have been replaced by hydrous phases. Rubin et al. (2007) prescribed a rating of CM2.2 to describe the extent of hydrous alteration. Howard et al. (2009) characterised the modal mineralogy of Nogoya using x-ray diffraction analysis. The authors reported modal mineralogy of Fe-cronstedtite (43-44%), Mg-serpentine (32-33%), olivine (15%), pyroxene (4%), magnetite (2.2%) with minor calcite, pentlandite and pyrrhotite.

Sutter's Mill- regolith breccia composed of CM2 lithologies

The Sutter's Mill (SM) chondrite represents a regolith breccia composed of CM lithologies that have experience variable aqueous alteration and thermal metamorphism (Jenniskens et al., 2012; Zolensky et al., 2012). Zolensky et al. (2012) reported ~3.2 % phyllosilicates in SM compared to 6 % in most CM chondrites. The matrix is mainly composed of fine-grained olivine with xenolithic materials typical of enstatite type chondrites (Zolensky et al., 2012). Uniform distribution of Na and K in SM2-4 suggests that the matrix of this sample did not experience aqueous alteration as opposed to the CM lithologies hosted in the matrix. A unique feature of the SM chondrite is that it contains both metamorphosed and non-metamorphosed CM components, this has not been reported in CM chondrites that have been studied previously (Zolensky et a., 2012).

Analytical methods

The petrography of the CV and CM chondrites was studied using back scattered electrons (BSE). BSE images were taken on the Zeiss EVO MA15 SEM (with OXFORD Instruments Aztec Synergy EDS/EBSD) at the MQ Geoanalytical (formerly GAU), in the Earth and Planetary Science (EPS) Department, Macquarie University, Sydney.

Neutron Computed Tomography – analysis

NCT analysis operates on the same principles as x-ray based computed tomography but uses a different imaging source i.e. neutrons instead of x-rays. Neutrons are electrically neutral particles and interact negligibly with the electric charge of electrons (Strobl et al., 2009). Neutron attenuation results from interaction of the incident neutron with the atomic nuclei by absorption or scattering (Suppli., Fig. 2.1a). This property of neutrons makes them especially sensitive to light elements such as hydrogen, Lithium and Boron. Because of this, neutron imaging techniques are particularly effective in determining the spatial distribution of hydrated mineral phases. At the same time, Ni and Fe exhibit relatively high attenuation coefficients (Suppli., Fig. 2.1, left).

NCT analyses were conducted using the neutron imaging instrument, DINGO, at the 20 MW Opal research reactor, ANSTO, Sydney (Suppli., Fig. 2.2a). This instrument uses thermal neutrons with a wavelength centred on 1.8 Å. The beamline characteristics are as follows; flux on sample of $1.15^{x}10^{7}$ n cm^{-2} s^{-1} and field of view = 20x20 cm. The collimator has two positions which allow for high resolution (Length (L) /Diameter (D) = 1000) and high speed (L/D = 250), the experiment was run using the high resolution setting (Suppli., Fig., 2.2b). Neutron projections were produced using a scintillator (50um thick ZnS/^{6}LiF screen) to convert neutrons into visible light which are then captured using an ANDOR IKON-L CCD camera and a Makro Planar 100mm lens with a field of view of 10x10 cm. This set up allowed for spatial resolution of 25 µm per pixel, giving a voxel (3D pixel) resolution of 25x25x25 μm^3. During the neutron tomographic scans, the samples were housed on a rotating stage and neutron projections were captured using rotations at equiangular steps of 0.576^{o} over 360^{o} with a 110s exposure time.

Micro Computed Tomography analysis

One sample, Allende, was imaged using micro-computed x-ray tomography to produce a comparative dataset. Micro CT analysis was done obtained on a Zeiss XRADIA MicroXCT-400 with beam conditions of 70KVp and 33µ. During data acquisition, 1500 projections were taken during a 360^{o} rotation of the sample. The integration time was 0.5s per projection with a spatial resolution of 25 µm. The analysis was conducted at the Australian Centre of Microscopy & Microanalysis, University of Sydney, Australia.

Visualisation and quantification

Raw greyscale images were stacked and decompressed using ImageJ software. Low attenuation signals are dark and high attenuation signals are bright in greyscale (Figure 2.3). The

data was additionally processed using a non-local means filter to reduce noise (Buades et al., 2005). During data reconstruction 2D images or slices are produced perpendicular to the axis of rotation, this provides a series of slices in the X, Y and Z axis. The reconstructed volume data for both x-ray and neutron scans were visualised in 2D slices and 3D volume renders using the Visualisation Sciences Group (VSG) Avizo Fire® software.

Quantification of chondritic components required segmentation based on grey scale intensity to produce a schematic 3D model (Fig. 2.1). Neutron tomography images were segmented allowing distinction of four components within the chondrites based on their attenuation co-efficient. These phases included; type I chondrules + refractory inclusions, matrix, high density and high hydration areas. Segmented phases were then quantified in terms of volume, size and distribution using VSG Avizo Fire®. Error analysis was conducted by completing multiple iterations of the segmentation. The main source of error comes from the migrating of boundaries between different components and resulted in a relative error of ~2 % for estimating the modal abundance. The relative abundance of Fe rich altered chondrules was estimated by visual counting. Due to the inability to adequately isolate intact chondrules from refractory inclusions and chondrule fragments, chondrule statistics for Allende, NWA3118 and NWA4502 (presented in Table 2.1) was obtained by quantitative analysis of BSE images using the ImageJ software (Rasband, 2012).

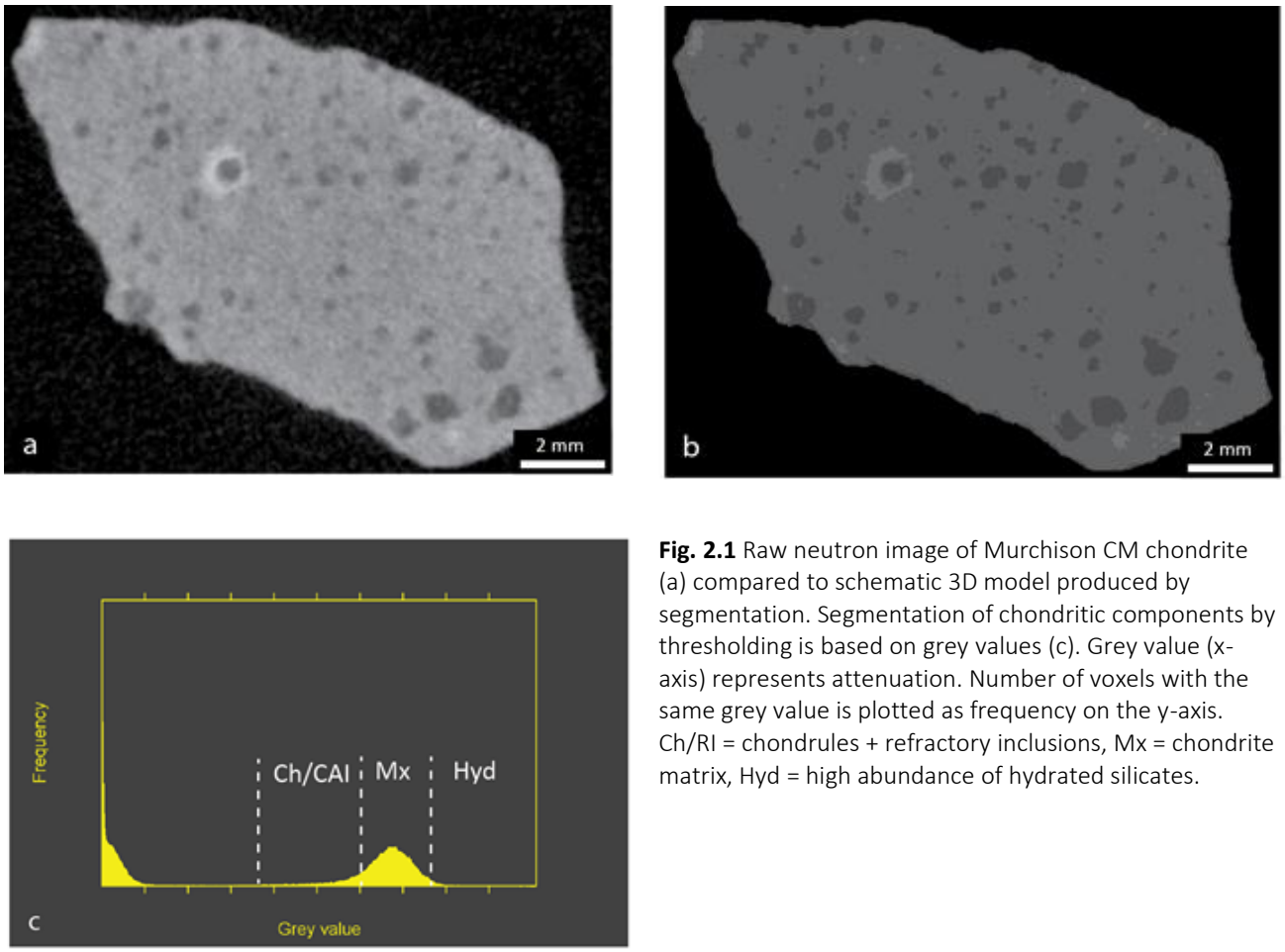

Fig. 2.1 Raw neutron image of Murchison CM chondrite (a) compared to schematic 3D model produced by segmentation. Segmentation of chondritic components by thresholding is based on grey values (c). Grey value (x-axis) represents attenuation. Number of voxels with the same grey value is plotted as frequency on the y-axis. Ch/RI = chondrules + refractory inclusions, Mx = chondrite matrix, Hyd = high abundance of hydrated silicates.

Results

Components in CV chondrites

Chondrules and refractory inclusions both have a low attenuation signal but differ in morphology i.e. chondrules are spherical whilst refractory inclusions can be spherical, elongated or amoeboid in shape. A distinctive chondrule and refractory inclusion seen in Figure 2.2b can clearly be linked in the 3D volume render (Fig. 2.2a). Prevalent chondrule alteration in Allende and NWA3118 results in the receding of the true chondrule boundary (Fig. 2.2c and 2.3a). Fe-rich sulphide, oxide and metals (referred to collectively as opaques) can clearly be distinguished within the chondrule interior but overlap with the signal of the matrix (Fig. 2.2).

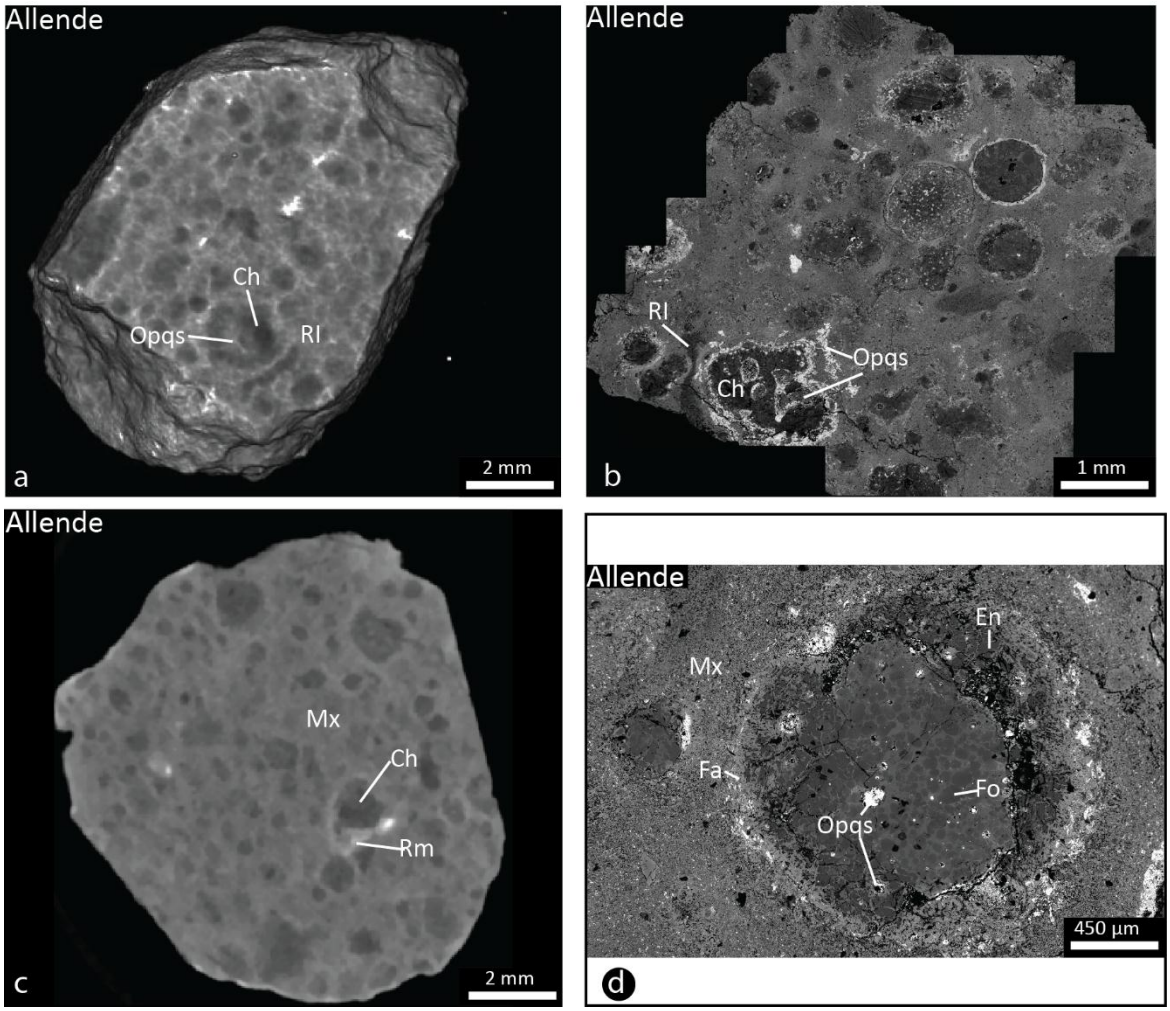

Fig. 2.2 3D volume renders of Allende displaying cut face (a) with corresponding BSE image of the cut section (b). Chondrules and refractory inclusions can clearly be correlated. Filtered neutron image of Allende (c) showing a high attenuation signal around one chondrule. BSE image of an olivine-pyroxene porphyritic chondrule with fine grained fayalitic olivine on the rim of the chondrule (d). Ch= chondrule, RI = refractory inclusion, Mx = chondrite matrix, Fo = forsteritic olivine, Fa = fayalitic olivine, En = enstatite, Opqs = troilite + magnetite, Rm = chondrule rim composed of low porosity fayalite rich olivine and opaques.

Many chondrules in NWA3118 exhibit a distinct rim with a higher attenuation signal compared to the matrix (Fig. 2.3). In some cases, these rims can be continuous between neighbouring chondrules (Suppli., Fig. 2.3). Similar rims are also observed around chondrules in Allende (Fig. 2.2) but show no connectivity (Suppli., Fig. 2.4). The attenuation signal of rims around chondrules in NWA3118 and Allende correlate with fine grained rims of Fe-Mg silicate material (predominately Fa-rich olivine) and progressively into the chondrule interior in NWA3118 (Fig. 2.3b). Fa-rich olivine in these rims has chemical compositions similar to matrix olivine and the boundary between the rim and matrix is always sharp. The most noticeable difference between rim and matrix grains is the porosity. The fine grained nature of the matrix and size of pores makes quantifying porosity using neutron imaging techniques difficult, however the loss of porosity is clearly observable in BSE images (Fig. 2.2d and 2.3d).

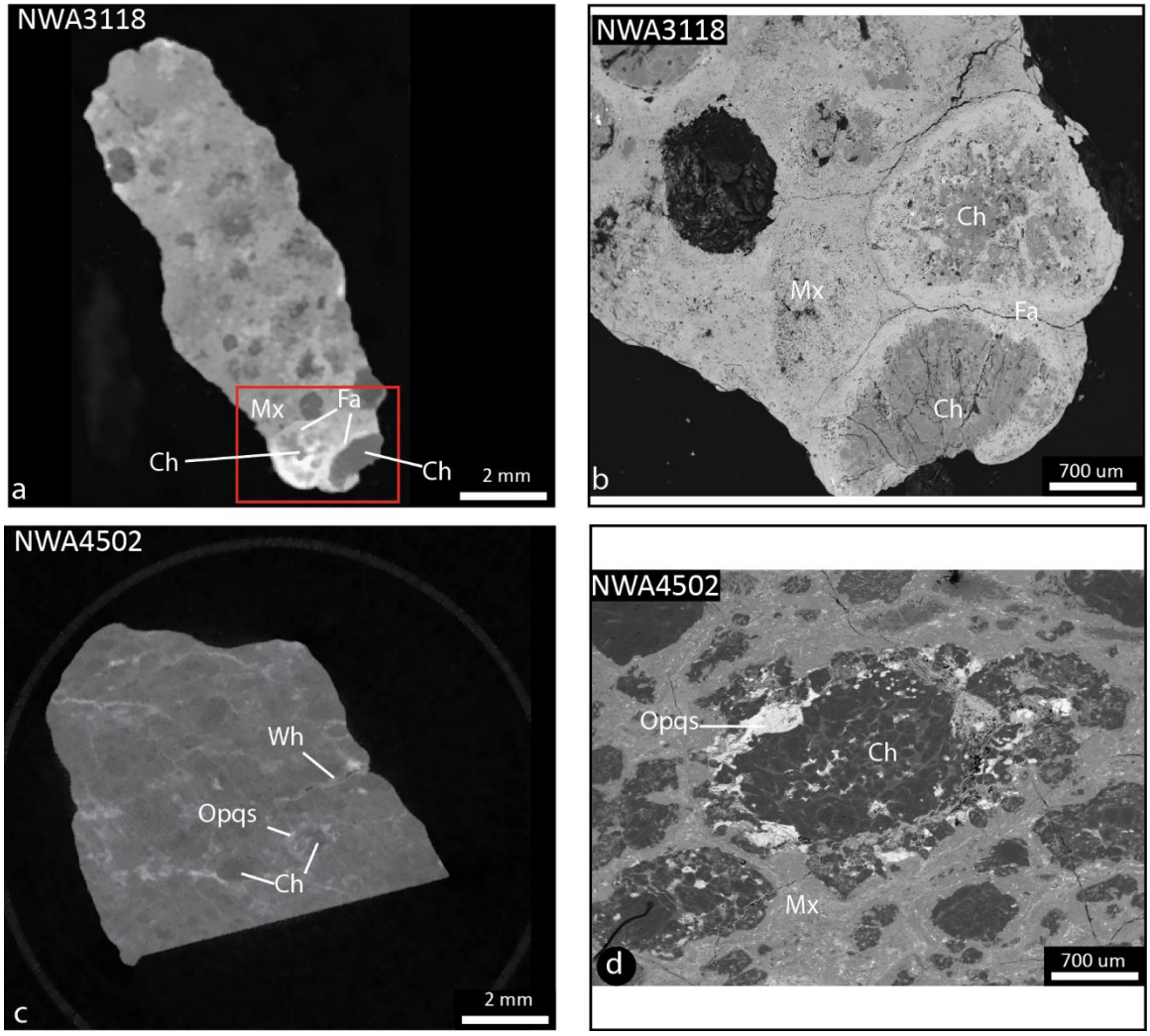

Fig. 2.3 Neutron image of NWA3118 (a) with corresponding BSE image (b) demonstrates that the high attenuation signal is related to fine-grain fayalitic olivine with little observable porosity. Variable porosity in the matrix may contribute to the heterogeneous attenuation signal observed in the matrix. High chondrule density in NWA4502 (c) makes distinguishing individual chondrules difficult. Fractures with Fe-oxide from terrestrial weathering is clearly visible and some chondrules are surrounding by material with a high attenuation signal. Chondrules in NWA4502 often contain an abundance of sulphides and Fe-oxides at the edge (d). Ch = chondrule, Fa = fayalitic olivine, Opqs = Opqs = troilite + magnetite, Mx = chondrite matrix, Wh = terrestrial weathering.

The high abundance of chondrules relative to matrix in NWA4502 makes resolving the individual properties difficult (Fig. 2.3c). The most notable petrographic features include Fe rich weathering along late stage fractures (Fig. 2.3c). Chondrules that are intersected by these fractures can have similar attenuation signals indicating some chondrules may have experienced terrestrial Fe weathering although similar features around chondrules distal to these fractures can be observed (Fig. 2.3c). The abundance of opaques surrounding chondrules (Fig. 2.5d) may also result in a high attenuation signal. Distinguishing between alteration and opaques is not always possible due to the overlapping attenuation signal and because individual chondrules are poorly resolved.

Both Allende and NWA3118 show attenuation gradients across the chondrite matrix. Variability in attenuation in the matrix is especially prevalent around chondrules (Fig 2.2 c and 2.3a). BSE images (Fig. 2.4b and 2.5b) reveal variable porosity in the matrix of Allende and NWA3118 with little noticeable change in mineralogy and chemistry. The matrix in NWA4502 represents a much smaller percentage of the sample (Fig. 2.3d). No significant attenuation gradient was observed in the NWA4502 chondrite matrix. Opaques in the matrix of NWA4502 and Allende cannot be resolved due to overlapping of the attenuation signal with fayalite.

Components in CM chondrites

Type I chondrules in the Murchison CM chondrite are distinguishable by their low attenuation signal (Fig. 2.4a). Several chondrules contained extended rims with a high attenuation signal (Fig. 2.4a). For comparison, Figure 2.6b shows a porphyritic olivine chondrule in Murchison surrounded by a fine-grained rim. These rims contain less visible porosity compared to the chondrite matrix. Discrete mm sized angular fragments with a similar attenuation signal to the fine-grained rims are also observed in the matrix (Fig. 2.4a). In 3D volume renders, areas of high attenuation in the matrix are discrete and not interconnected (Suppli., Fig. 2.5). The attenuation signal of the chondrite matrix in Murchison is variable, albeit to a lesser extent compared to Allende and NWA3118.

The Nagoya CM sample is predominately composed of matrix with minor amount of chondrules and refractory inclusions. The most distinct feature of this sample is the presence of clasts exhibiting a high attenuation signal (Fig. 2.4c). In BSE images, the largest hydrated clast is clearly distinguishable from the background matrix (Fig. 2.4d). In 3D volume renders, these clasts are discrete and appear to be non-spherical and sub-rounded (Suppli., Fig. 2.6). Based on neutron imaging, the clasts are internally homogenous (Fig. 2.4c). However, BSE images of the hydrated clast (Fig. 2.4d) show that the clasts are comprised of serpentinised chondrules <500 μm diameter with a phyllosilicate rich interstitial matrix.

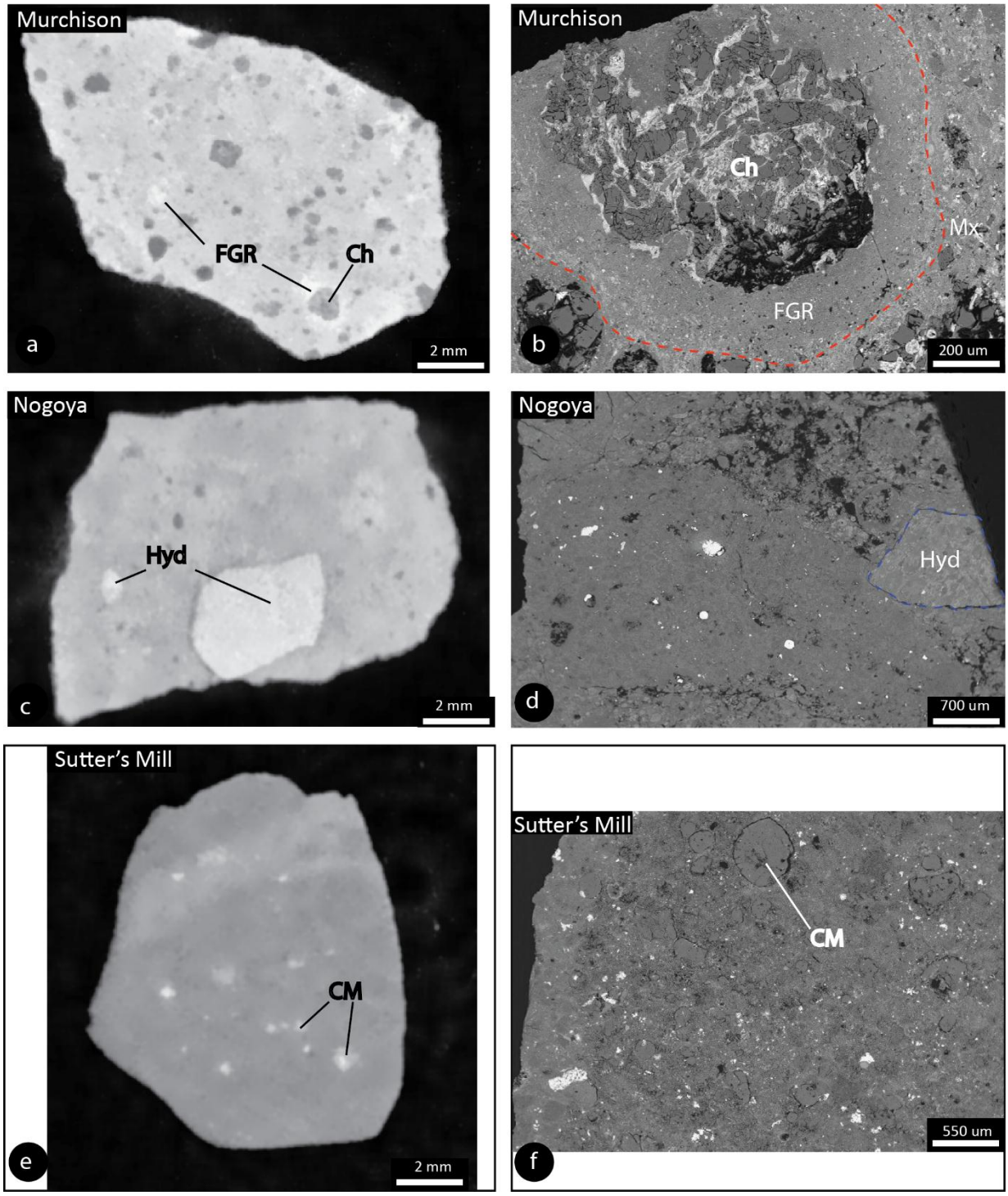

Fig. 2.4 Filtered neutron images of (a) Murchison, (c) Nogoya and (e) Sutter's Mill compared to BSE images (b, d & f). Areas of high attenuation around chondrules in Murchison (a) correspond to fine grained rims (outlined in red). A large clast seen in (c & d) can clearly be distinguished from the surrounding matrix. Ch = chondrule, Mx = chondrite matrix, FGR = fine grained rim, Hyd = hydrous clast, CM = CM lithology.

The Sutter's Mill CM chondrite is mostly comprised of matrix with a lower attenuation signal compared to Nogoya and Murchison (Fig. 2.4e). As noted by Zolensky et al. (2012) the matrix itself does not contain a high abundance of phyllosilicates. Abundant Fe, Ni sulphides in the matrix (Fig. 2.4f) are not resolved in the neutron images (Fig. 2.4e). Notable variation in

attenuation across the matrix forming a band like feature (Fig. 2.4e) is not observable in BSE images. Almost all Sutter's Mill samples were exposed to rainfall before recovery (Jenniskens et al., 2012). This makes interpreting this hydrated band as a 'primary' feature dubious. Spots of high greyscale intensity are found throughout the sample as millimetre sized fragments or as mm sized spherical objects morphologically like chondrules. 3D imaging shows that these high attenuation spots are discrete and have no interconnectivity (Suppli., Fig. 2.7a). These likely represent CM lithologies distributed with an olivine rich matrix. Chondrules were distinguishable by morphology but are difficult to distinguish from the matrix in BSE images (Fig. 2.4f).

Quantification of chondrite components

Table 2.1 Modal abundance of chondrite components obtained by segmentation in this study (Vol.%). Chondrule properties are measured from 2D sections. **Relative abundance of Fe rich alteration is based on visual counting.

	Allende	NWA3118	NWA4502	Murchison
Chondrite components				
Type I Chondrules + RI's	34	25	55	14
Matrix	60	68	36	83
Fe rich opaques + low porosity fayalite	5	7	9	
Phyllosilicate rich fine grained rim				3
Total	99	100	100	100
Chondrule + RI's/matrix	0.57	0.37	1.52	0.17
Chondrule properties				
Average diameter (mm)	0.570	0.892	0.934	
Max diameter (mm)	1.796	1.939	2.883	
Min diameter (mm)	0.138	0.192	0.314	
Average aspect ratio	1.31	1.31	1.73	
Relative abundance of Fe-rich alteration*	80	96	20	

3D modal abundances of chondrite components for Allende, NWA3118, NWA4502 and Murchison based on segmentation models is presented in Table 2.1. Quantification of the components in Nagoya and Sutter's Mill CM chondrites are not reported due to large error margins from the overlapping of chondrule and matrix attenuation signal. In the CV chondrites, NWA4502 had the greatest chondrule + refractory inclusions /matrix ratio at 1.52; followed by Allende 0.57 and NWA3118 0.37. Murchison had a measured chondrule + refractory inclusions/ matrix ratio of 0.17 in comparison. The percentage of Fe-rich altered chondrules in the CV chondrites increased with the modal percentage of matrix (Table 2.1). The average chondrule diameter decreased from 0.934 NWA4502 to 0.892 in NWA3118 and 0.570 in Allende. NWA4502

recorded the greatest size distribution with diameters ranging from 2.883 mm to 0.314 mm. NWA4502 also contained the least spherical chondrules with an average aspect ratio of 1.73 compared to 1.31 for Allende and NWA3118.

Comparison between NCT and micro CT scanning

Micro CT scanning was conducted at the same spatial resolution to produce a comparative data set. Chondrules and refractory inclusion are clearly distinguished by their low attenuation signal and morphology (Fig. 2.5). Chondrule and refractory inclusions are equally distinguishable in NCT scans, however the boundaries appear less sharp (Fig. 2.5b). Fe-rich altered chondrules are easily recognised using micro CT scanning; they appear as dark cores mantled by material with a slightly higher attenuation signal (Fig. 2.5). Apart from the enhanced clarity in observed in the micro CT scan, opaque minerals are easily distinguishable from fayalite rich alteration. Opaques which include magnetite and troilite can be seen forming rims around chondrules and in the interior as small blebs (Fig. 2.5a). However, in NCT subtle variations within the matrix are detectable, which are less apparent in the micro x-ray CT scan.

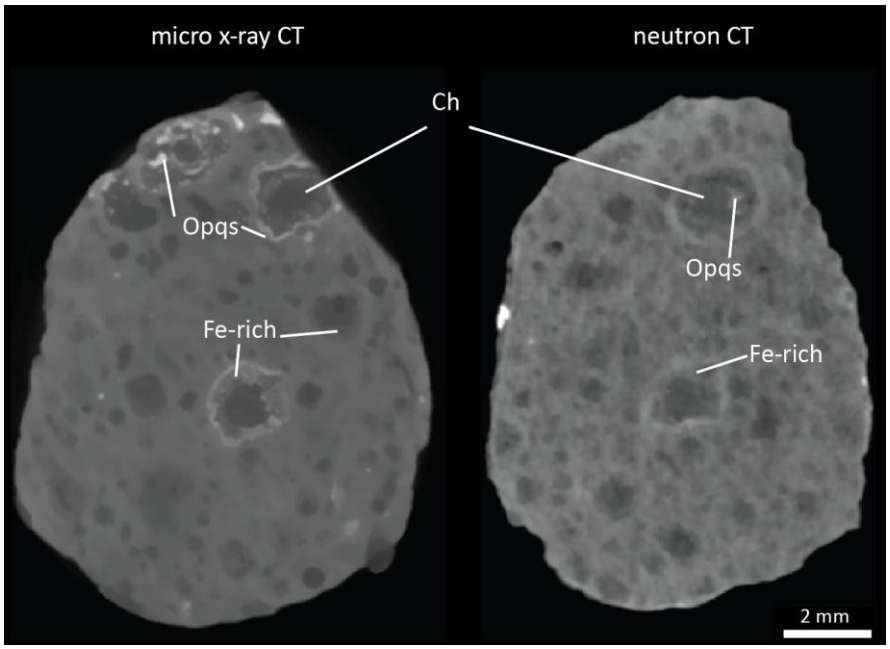

Fig. 2.5 Comparison of micro CT scan (left) and neutron CT scan (right). Ch = chondrules, Opqs = magnetite + troilite, Fe-rich = Fe-rich alteration.

Discussion

Differences in petrography of CV and CM chondrites: Implications for geological processes occurring on small planetary bodies

Chondrules across the three CV chondrites studied demonstrated variability in the attenuation signal in the chondrule interior. When compared to BSE images, this reflects the

abundance of opaques and the extent of Fe-rich alteration in the chondrule interior. Alteration of chondritic components in oxidised Allende style chondrites is commonly attributed to fluid-assisted thermal metamorphism occurring above 200^{o}C on the chondrite parent-body (Krot et al., 1998, 2000, 2001, 2004). The resultant formation of fayalitic olivine responsible for the high attenuation signals in neutron images occurs by several different mechanisms such as; replacement of enstatite and magnetite, Fe-Mg exchange between olivine and fluid as well as direct precipitation (Krot et al., 2004). The high percentage of chondrules exhibiting Fe-rich alteration indicates that this was a prevailing process on the Allende and NWA3118 chondrite parent body.

Allende and NWA3118 contained a progressively higher modal abundance of matrix and Fe-rich altered chondrules compared to NWA4502. The relationship between aqueous alteration and matrix can be observed between CV and CM chondrite groups. The CM chondrites analysed in this study consistently contain less chondrules and more matrix then the CV chondrites. This relationship between modal matrix abundance and the prevalence of altered chondrules suggests that the process of aqueous alteration is implicit in the formation of matrix grains. In a study of the Mokoia CV chondrite, Tomeoka & Ohnishi (2015) proposed that matrix grains may have formed by disaggregation of matrices from wet and dry regions as well as abrasion and grinding of chondrules/rims during fragmentation and transportation in fluidised state.

Allende and NWA3118 demonstrated variation in the attenuation signal across the matrix. The mineralogy of the matrix is mostly homogenous across both samples but there are notable differences in grainsize and porosity in BSE images. Variable attenuation in the matrix likely reflects variable porosity. The matrix around chondrules demonstrates the most variation in attenuation. Similarly, fayalite rich rims around chondrules in NWA3118 were sometimes found to be continuous (Suppli., Fig. 2.3). Based on the model previously outlined, the surrounding matrix and chondrule can be viewed as a separate clast from a different source region. The exact nature of variation within the chondrite matrix remains ambiguous. Forman et al. (2016) conducted an EBSD analysis of the Allende matrix and observed that high degrees of crystal-plastic deformation was spatially heterogeneous. They concluded that Allende experienced locally heterogeneous stress and temperature conditions because of impact processing. This study provides a viable mechanism for heterogeneous matrix compaction. Reduction in porosity may also result from a change in grainsize i.e. smaller grains will produce less porosity. In comparison, Murchison and Nogoya demonstrated a considerably more uniform attenuation signal in the matrix. This initially

suggests that the CM chondrite matrix is more homogenous, however the abundance of phyllosilicates in the matrix of CM chondrites may make NCT less sensitive to changes in porosity.

High attenuation signals in the Murchison CM chondrite are observed as halos around chondrules and as discrete angular clasts dispersed in the matrix. Zolensky et al. (1993) reported an abundance of hydrous minerals including; serpentinite, saponite and tochilinite in fine grained rims surrounding chondrules in Murchison. CM alteration occurred at low temperatures, up to 80^{o}C (Baker et al., 2002). Fine-grained rims around chondrules are thought to have formed by two main mechanisms. Early authors attributed the fine-grained rim to accretion of dust onto the chondrule in the solar nebula (King & King, 1981; Hua et al., 1996). Fine-grained rims have been proposed to represent original matrix around the chondrule forming a 'clast' which is subsequently transported to form the source region (Tomeoka & Ohnishi, 2010; Takayama & Tomeoka, 2012). In this scenario, fine-grained rims can be viewed as more strongly hydrated matrix from a different source region. The observation that not all chondrules contain these rims, and similar material can be found as discrete clasts in the matrix support the parent body formation. Most notable is the appearance of sub-rounded angular hydrated clasts in the Nagoya CM sample (Fig. 2.4c). These clasts record a higher hydration signal compared to the matrix and can clearly be identified in BSE images. The appearance of hydrated clasts in Nagoya provides the most compelling evidence for fragmentation and transportation of material from different source regions on the chondrite parent body.

A model for the formation of CM and CV chondrite lithologies

A simplified model for the formation of the CM and CV chondrite lithologies observed in this study is presented (Fig. 2.6) and builds upon the work of Tomeoka & Ohnishi (2015). The precursor lithology to both CV and CM chondrites is interpreted to be a pristine CV chondrite. NWA4502 represents an approximation of this precursor lithology based on the high abundance of chondrules relative to matrix and the relatively little alteration present. Alteration of the precursor material takes places in different source regions. In each source region alteration is fluid mediated, the primary difference between CM and CV chondrites is temperature. In low temperature source regions (source region A), the abundance of H results in the hydration of Fe-Mg silicates to form hydrous silicates such as serpentinite and saponite (McSween, 1979). In high temperature source regions (source region B), fluid meditated thermal metamorphism is dominated by Fe-Mg exchange (Krot et al., 2000). The Mokoia CV chondrite contained chondrule with phyllosilicate rich

veins whilst the matrix showed no evidence of aqueous alteration (Tomeoka & Ohnishi, 2015). This suggests that in the same chondrite parent body source regions both CM and CV can occur on.

Altered lithologies are subsequently fragmented by impacting to produce clasts of chondrules and matrix. The diversity of CV and CM lithologies reflects the relative abundance of material from different source regions. For example, Murchison is predominately source region B with some input from source region A. The roundness of chondrule rims in both CV and CM chondrites suggest that fragmented clasts were subjected to motion induced frictional smoothing during transportation. A plausible mechanism to round angular fragments during transportation is by impact induced granular flow. Impacting in the early solar system was a common occurrence (Kring & Cohen, 2002) and therefore multiple impacts may be enough to frictionally smooth particles. This process may have not been too dissimilar to pebble rounding in streams. The low gravity environment could imitate several properties of particle behaviour in a viscous fluid. For example, agitated particles can be suspended, bump into each other and settle.

Another possible mechanism of rounding could be aeolian transport. Aeolian systems are common in the solar system, for example the surface dynamics on Mars is predominately governed by aeolian systems (Calder et al., 2000). Furthermore, large areas of Saturn's moon Titan were found to be covered in linear dunes (Lorenz et al., 1995). The main problem with aeolian transportation as the mechanism for rounding particles is whether the chondrite parent body was sufficiently large enough to sustain a dynamic atmosphere. Based on the conditions for pore water convection, Young et al. (2003) provided a theoretical maximum diameter of 80km for the chondrite parent-body, too small to retain enough atmosphere. This however may not be a prerequisite for aeolian transport to occur. Transient atmospheres can be formed near the surface of small planetary bodies (Moon, Mercury, asteroids etc.) by impact vaporisation (Nemtchinov et al., 2002). This phenomenon has even been observed on the Moon (Potter & Morgan, 1988).

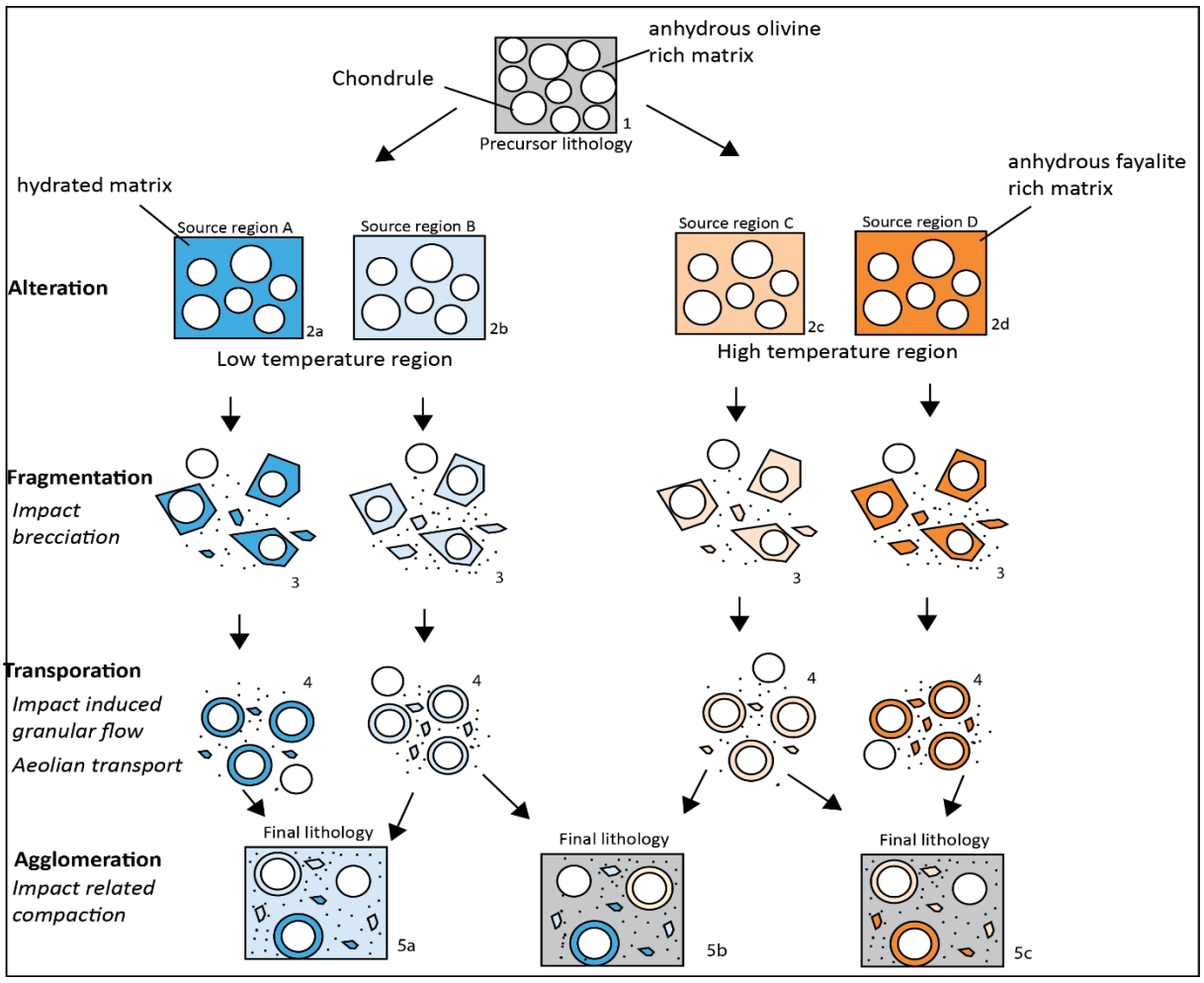

Fig. 2.6 Schematic model for the formation of the final CM and CV chondrite lithology observed in Murchison and Nogoya. Stage 1: Precursor lithology is inferred to be analogous to CV chondrite with chondrules set in a fine-grained olivine rich matrix. Stage 2: Alteration takes place in low temperature and high temperature regions. Stage 3 represents fragmentation where chondrules and surrounding matrix are fragmented into clasts. This process also produces matrix grains. As seen in Nogoya, this can also produce larger blocks containing multiple chondrules. Chondrules are then transported in Stage 4. During this process, chondrule rims are rounded, the process of abrasion creates more matrix grains. Stage 5 represents agglomeration of the different components. 5a and 5c represents the lithology observed in Murchison and Allende. Respectively. 5b is a mix of CM and CV components as seen in the Mokoia CV chondrite (Tomeoka & Ohnishi, 2015).

Use of neutron tomography in the study of chondrites

The CV chondrites selected are nominally anhydrous and discrimination between chondrules + refractory inclusions, matrix and Fe rich opaques + low porosity fayalite results from the distribution of Fe and porosity. In comparison, CM chondrites contain an abundance of hydrated silicate minerals and phase segmentation would result from the combination of Fe and H distribution as well as porosity. In the CM chondrites NCT permitted the discrimination between chondrules + refractory inclusions, matrix and a high attenuation phase. In the Murchison chondrite, this signal correlates with fine-grained rims around chondrules. In the study of CV chondrites, micro CT can resolve magnetite and troilite from fayalite rich alteration. The resolution of opaque phases as seen in micro CT scans likely permits detailed visualisation and quantification.

micro CT scanning would also be effective in comparing the distribution of Fe and H in CM chondrites, thus clarifying the origin of high attenuation signals in these chondrites.

NCT is effective in studying the 3D distribution, shape and connectivity of components in the CV and CM chondrites. In NWA3118 fayalite alteration rims around was seen to be continuous around one group of chondrules. In both Murchison and Allende, high attenuation rims around chondrules showed no connectivity between neighbouring chondrules. Similarly, the distribution and geometry of mm sized clasts in the Murchison chondrite matrix was visualised (Suppli. 2.4). Neutron tomography gave a unique 3D visualisation of hydrated clasts in Nogoya. Importantly, features such as roundness, sphericity, sized and relative abundance of hydrated silicates in the clasts could be determined. In the Sutter's Mill chondrite, CM lithologies were distinct from the matrix and could be visualised effectively. A continuous band of hydration was resolved and imaged in 3D. Though the origin of this feature as a parent-body processes or terrestrial weathering was not established, it highlighted the strength of using NCT in mapping the distribution of H.

Allende and Murchison have been well studied over the last few decades in 2D sections and the petrography of each sample is well known. Ebel et al. (2009) calculated the modal abundances of a 121 cm^2 slab of Allende using x-ray image analysis and reported 38 vol. % for chondrules + CAI's and 61 vol. % for the matrix in Allende. Based on neutron imaging, the modal percentage of matrix and chondrules + CAI's in Allende was 34 vol. % and 60 vol. %. In the Murchison sample, this study estimated the modal abundances of chondrules + CAI's and matrix at 18 vol. % and 78 vol. %. McSween (1979) reported the modal abundances of chondrules + CAI's and matrix in Murchison at 24 vol. % and 64 vol. % respectively.

Segmentation and quantification of the petrographic components using neutron tomography permitted a good approximation of the modal abundance of type I chondrules + CAI's and matrix in CV chondrites. In comparison, the modal abundances calculated for Murchison was significantly different to the reported modal abundances by McSween (1979). The likely reason for this is that the hydration of chondrules would give the same attenuation signal as the matrix and segmentation is predominately based on greyscale thresholding and not morphology. Thus, neutron imaging-based quantification led to an overestimation of the matrix and underestimation of the chondrule population in hydrated chondrites. In both CM and CV chondrites, the abundance of opaques cannot be accurately quantified as the attenuation signal overlaps with; low-porosity fayalite and hydrous phases.

Conclusion

Based on the quantification and visualisation of CM and CV chondrite components we propose that CM and CV lithology formed by the following processes: (1) fluid mediated alteration of a pristine CV like chondrite precursor at low and high temperatures. Source regions are characterised by different alteration style and intensity of alteration. (2) Impact driven fragmentation produced clasts consisting of matrix and chondrule from different source regions. (3) Clasts from different source regions were frictionally smoothed during transportation (4) Agglomeration through impact related compaction forming the final lithology. We suggest granular flows mediated by multiple impacts or aeolian transport in transient impact generated atmospheres as possible transport mechanisms.

3D visualisation and quantification of CM and CV chondrites using neutron tomography provides a unique look at the structure of chondrites whilst maintaining the samples integrity. The major drawbacks of neutron tomography include the relatively low resolution for studying chondrites and the inability to isolate hydrous phases. These drawbacks can be overcome by conducting complementary μCT studies which will allow the accurate distribution of H to be derived. Neutron tomography in combination with μx-ray CT scanning and 'classic petrography' promises to be a powerful tool for the investigation of meteorites due to the following reasons;

i. Combined neutron and μx-ray CT can be used to accurately map the distribution of hydrous and metallic phases in three dimensions. Though classic petrography is useful in assisting with correlating attenuation with the true petrography, it is not necessary when both imaging techniques are combined. This is particularly useful for rare and precious meteorite samples.
ii. Chondrite components can be visualised in three-dimensions. This allows for a more complete understanding of the spatial relationships between different components to be made.
iii. 3D petrography can be accurately quantified using neutron tomography on anhydrous samples. Hydrated samples will require a complementary μx-ray CT study to accurately quantify the abundance of matrix and chondrules.

Chapter 3

Textural and chemical evolution of chondrules in CV_{oxA} chondrites: implications for nebular source regions and geological processes on small planetary bodies.

Abstract

Carbonaceous chondrites are unique in that their individual components record processes occurring in the early solar nebular and on small planetary bodies. It is pivotal that the subsequent modification of these components is understood. In this study, the chemical and textural characteristics of the three CV_{oxA} chondrites Allende, NWA3118 and NWA4502 are studied. A new chondrule classification scheme is firstly presented, based on mineral textures and their modification through planetary processes. This classification is used to develop a refined model where the variability in textural and chemical signatures seen in chondrules is used to illuminate the processes of nebular gas-chondrule interaction and chondrite agglomeration.

Introduction

Carbonaceous chondrites are relict material left over from the earliest stages of our solar system's formation and are composed of primary nebula condensates (refractory inclusions) and Fe-Mg igneous silicate spherules (chondrules) set within a fine-grained matrix (Grossman et al., 1988). They provide a unique record of the astrophysical and geological processes occurring in the early solar system as well as insights into the formation and accretion of the first solids through to the geological evolution of small planetary bodies (Ringwood; 1966; Wasson, 1985; Wasson & Kallemeyn, 1988). Although carbonaceous chondrites are primitive, little recovered chondritic material contain a pristine record of the early solar system unaffected by secondary processing in the early solar nebular or on the chondrite parent body (McSween, 1987; Bischoff, 1998). Understanding the extent and nature of alteration in carbonaceous chondrites is pivotal for two reasons; i) deciphering the primary 'nebular' signature from later alteration is vital in accurately constraining the physical and chemical conditions of the early proto-planetary nebular ii) subsequent metasomatic and metamorphic alteration of the primary chondrite body provides important insight into geological processes occurring on small planetary bodies during planetary formation. Such processes may be occurring on other planetary bodies in the solar system now, albeit on a smaller scale.

Chondrules are the most recognisable and abundant petrographic component of chondrites. A comprehensive classification of chondrules based on their textures and mineral modes (Suppli., Table 3.1) was presented by Gooding & Keil (1981). A complementary

compositional classification scheme was produced by McSween (1977) and Scott & Taylor (1983) which divides chondrules in to Type I and II based on the bulk FeO content (Table 3.1b). Type I chondrules contain FeO poor olivine and pyroxene with enstatite composition. Type II chondrules contain FeO rich olivine and pyroxene. The two main categories are further sub-divided into A and B based on the relative abundances of olivine and pyroxene

The established interpretation of chondrule formation involves the rapid heating of dust balls within minutes to hours during transient high temperature heating events in the proto-solar nebula around 4.5-4.6 billion years ago (Grossman, 1988; Amelin et al., 2002). Subsequent cooling results in the crystallisation of olivine and pyroxene with the residual refractory rich melt quenching to form glass or fine-grained pyroxene and plagioclase (Wood, 1963; Hewins, 1988). In this simplified closed system, chondrule bulk composition is entirely inherited from the precursor material (Hezel & Palme, 2007). However, there are several chondrule properties which support a more complex and dynamic pathway to chondrule formation (Krot et al., 2009). The chemical composition of chondrule glass, bulk composition of type I chondrules and mineralogical zoning of Low-Ca pyroxene around olivine cores was used as evidence by Libourel et al. (2006) to show that type I chondrule experienced open system melting. Marrocchi & Libourel (2013) suggests that the porphyritic olivine chondrules evolved to porphyritic pyroxene chondrules by progressive interaction with Si rich nebular gas instead of solely inheriting their composition from the chondrule precursor material.

The latter suggestion of a chemical evolution of chondrules is especially interesting in view of the major secondary minerals reported in CV chondrites. The oxidised Allende like CV group (CV_{oxA}) is unique in the style of secondary mineralisation that is present. These include ferrous olivine (Fa_{30-50}), magnetite, nepheline, sodalite, Ni-rich metal and Fe, Ni sulphides (Brearley & Krot, 2012). Kimura & Ikeda (1995) observed that the extent of alteration is highly variable and peripheral parts of chondrules are always more altered than the cores (Kimura & Ikeda, 1995). Krot et al. (1998, 2000, 2004) proposed that CV_{oxA} chondrites have been subjected to fluid assisted thermal metamorphism >200^{o}C. This process resulted in the dissolution and replacement of primary minerals, direct precipitation of secondary minerals along with the mobilisation and redistribution of Ca, Si, Fe, Mg, Mn, Na, and S by a fluid phase. The formation mechanism for ferrous olivine in this model includes; replacement of magnetite, replacement of enstatite, Fe-Mg exchange between olivine and fluid and direct precipitation from fluid (Krot et al., 2004).

The textural and chemical variability of the chondrules themselves as well as their mode of alteration has been mainly studied petrographically and chemically, however such differences would be expected to go hand in hand with distinct microstructural features and/or changes. Quantitative microstructural analysis using Electron Backscatter Diffraction (EBSD) combined with chemical analysis has proven to be a helpful tool in deciphering both earth and extra-terrestrial materials (Prior et al. 1999, Smith et al. 2015). Recently, replacement and reaction as the result of fluid/melt – rock interaction has gained considerable interest in the geological community (e.g. Putnis 2009, Stuart et al. 2016) and criteria for their recognition are been established. In this study we aim to constrain the textural and chemical evolution by nebular and parent-body processes using a combined chemical and microstructural approach. Here we concentrate on the geochemistry, mineralogy, texture, and microstructure of chondrules from three selected CV_{oxA} chondrites namely Allende, NWA4502 and NWA3118. To be able to rigorously document the degree of alteration and chemical changes a modified chondrule classification scheme is presented. Subsequently, the microstructures and chemistry from selected, representing chondrules which have undergone variable levels of nebular gas interaction and parent body alteration is provided.

Sample selection and descriptions

Three chondrites from the CV_{oxA} group were chosen for this study including one well known chondrite, Allende, and two lesser known samples; NWA3118 and NWA4502. Recent analysis using Neutron computed tomography (Chapter 2) shows that the three samples record a progressive decrease in the volume of chondrules (Table 3.1) where NWA4502 has the highest volume with 55 % and NWA3118 the lowest (25 %). A change in the volume percent of chondrules was found to be associated with alteration (Chapter 2). Under the assumption that a decrease in discernible chondrules represents an increase in post-chondrule formation alteration, the three chondrites selected represent a progression of alteration. The selected sample set provides a unique opportunity to investigate how the chemistry and microstructure of the different chondrite components, specifically chondrules, change with increasing alteration on the parent body.

Table 3.1 Modal abundances of chondritic components obtained by segmentation (vol. %). Chondrule properties are measured from 2D section. *Relative abundance of chondrules with Fe-rich alteration is based on visual counting. RI's = refractory inclusions.

	NWA3118	Allende	NWA4502
Chondrite components			
Type I Chondrules + RI's	25	34	55
Matrix	68	60	36
Fe-rich alteration + opaques*	7	5	9
Total	100	99	100
Chondrule + RI's/matrix	0.37	0.57	1.52

NWA 3118 was recovered in 2013 with an original mass of ~5.9 kg and described as having a low weathering grade (Akos et al., 2014). It is composed of type I chondrules and chondrule fragments, refractory inclusions, and matrix. Most chondrules surveyed are spherical with diameters ranging from 0.3 to 2 mm. Chondrules are predominately olivine with the rest composed of orthopyroxene, plagioclase, and opaque minerals (magnetite, chromite & troilite) (Fig. 3.1c, d). Sulphides and iron-oxides are observed to be entirely or almost entirely altered to fayalite. They are found as spheroidal droplets poikilitically enclosed in pyroxenes and in the chondrule groundmass. The fine-grained meteorite matrix is mainly composed of um sized euhedral fayalitic olivine platelets with clinopyroxene, nepheline, sodalite, Ti-Al-pyroxene and minor anorthite.

Allende is composed of chondrules, matrix, refractory inclusions, and opaque minerals. Chondrules in Allende range in size from 0.01 mm-3.2 mm in diameter and are generally found to be spherical (Fig. 3.1a), though some can take non-spherical irregular forms (Fig. 3.1b) with other found as fragments disseminated in the matrix (Fig. 3.1a and 3.1b). The major mineral chondrule constituents include olivine (forsterite to Fe-rich forsterite), enstatite and Ca-rich plagioclase. Minor mineral phases reported in previous studies include; kamacite, taenite, troilite, mackinawaite, antigorite, majorite, pentlandite, magnetite and anorthite (Kornacki & Wood, 1984). Chondrules surveyed in Allende contain olivine of predominately forsterite composition. The meteorite matrix in Allende is described as been a fine-grained porous aggregate of minerals including; euhedral fayalitic olivine platelets, clinopyroxene, nepheline, sodalite, Ti-Al-pyroxene and minor feldspars (anorthite) (Kornacki & Wood, 1984).

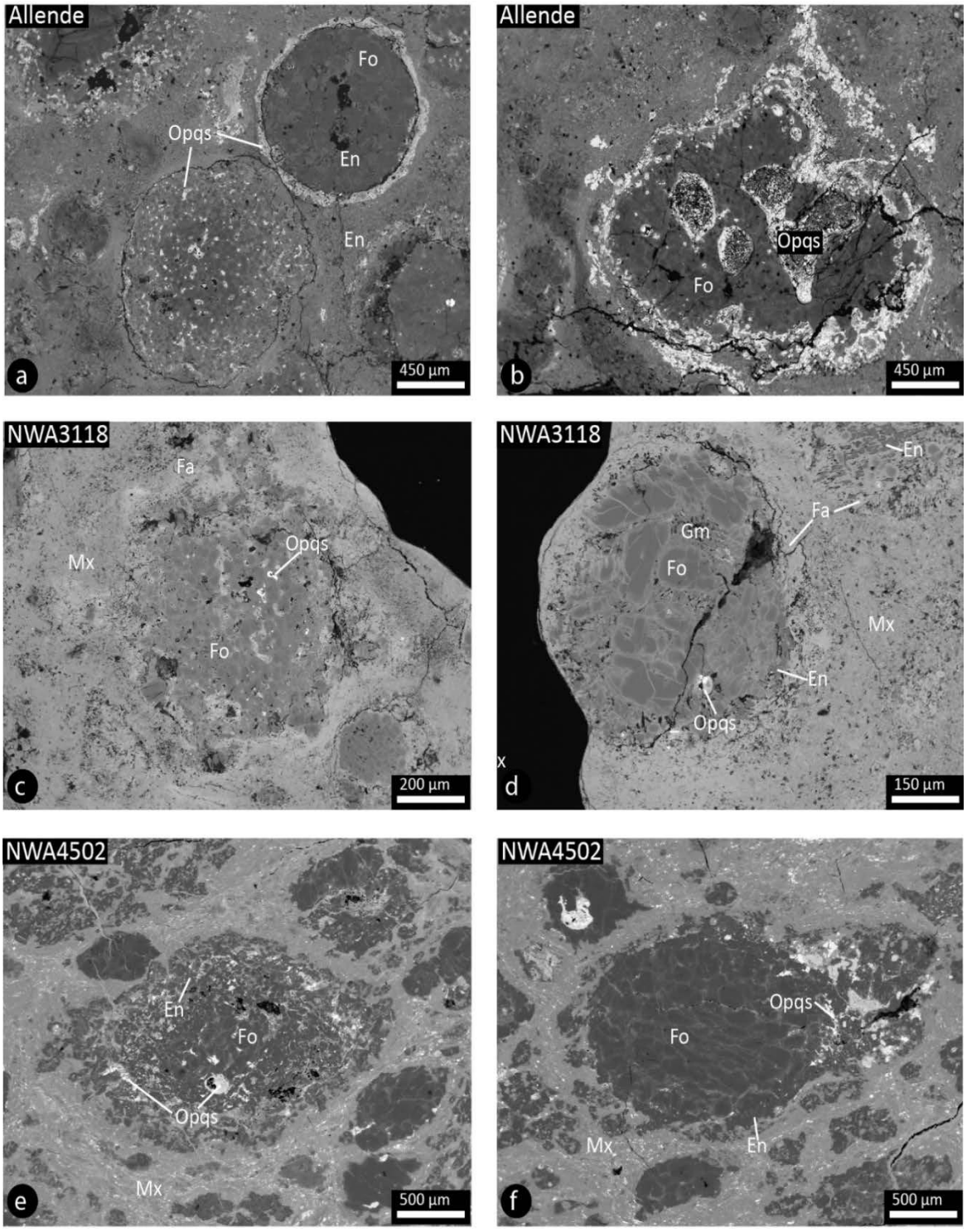

Figure 3.1 BSE images of PO chondrule with Fe zoning towards the edge and a PP chondrule with an Fe, Ni sulphide + magnetite rim in Allende (a). Irregular shaped PO chondrule with Fe, Ni sulphide + magnetite rim from Allende (b). PO chondrule with fayalite rich olivine replacing the chondrule groundmass and enstatite from NWA3118 (c). PO olivine chondrule from NWA3118 (d) with Na rich altered groundmass in the core and Fa rich olivine replacing enstatite on the rim. Opaques are altered to fayalite rich olivine. PP chondrule with olivine rich core from NWA4502 (e). Sulphides are abundant in the pyroxene rich zone. PO chondrule with minor enstatite at the edge (f). Fo = forsteritic olivine, Fa = fayalitic olivine, En = enstatite, Aug = augite, Gm = chondrule groundmass, Mx = chondrite matrix, Opqs = magnetite + troilite.

NWA 4502 is composed of well-defined chondrules and chondrule fragments and refractory inclusions hosted in matrix. NWA4502 has characteristics of weathering grade 1 exhibiting small oxide rims around metals and small oxide veinlets (Wlotzka et al. 1993). Chondrules surveyed in NWA 4502 are composed of forsteritic olivine and enstatite. Chondrules in NWA4502 are found to be predominately ovoid in shape (Fig. 3.1e, f). Diameters of intact chondrules range from 0.1 mm to > 4 mm. The majority of chondrules were also observed to contain an abundance of sulphides and iron oxides (Fig. 3.1e, f). They are found as a) massive blebs of troilite (+ magnetite) inter grown with pyroxene at the edge of chondrules, b) spheroidal droplets poikilitically enclosed in pyroxenes and c) amorphous pools located in the chondrule groundmass. The matrix of NWA 4502 is a fine grained porous aggregate of minerals dominated by µm sized fayalitic olivine as well as µm to mm sized grains of troilite, pentlandite and magnetite. Sapah (2016) reported rare alteration products typical of the CV3 Allende-like oxidised sub- group such as µm sized nepheline crystals and Fe-Ca rich silicates.

Analytical Techniques

The mineralogy and petrography of Allende, NWA3118 and NWA4502 was studied using back scattered electrons with the Hitachi desktop SEM and the Zeiss EVO MA15 SEM. Multi element EDX mapping (Mg, Si, O, Fe, Ni, S, Na, Ca, and Al) was done using the Zeiss EVO MA15 SEM (with OXFORD Instruments Aztec Synergy EDS/EBSD) at MQ Geoanalytical (formerly GAU), in the Earth and Planetary Science (EPS) Department, Macquarie University, Sydney. After the acquisition of each map, Si, Mg, Al, Ca, Na, Fe, Ni and S were combined into a single image to highlight the mineralogical characteristics of each chondrule which primarily included olivine, low Ca-pyroxene, Fe-Ni metals/oxides, sulphides and Ca- Al rich groundmass. The degree of parent body alteration observed in individual chondrules is measured as a function of the area percentages of altered groundmass and replacement of clinoenstatite by Fe-rich olivine.

Quantitative analysis of the mineralogical composition of chondrules was done using energy dispersive spectroscopy (EDS) on the Zeiss EVO MA15 SEM at MQ Geoanalytical, in the Earth and Planetary Science (EPS) Department, Macquarie University, Sydney. The EDS analysis was conducted under the following operating conditions; 15KeV accelerating voltage and 20nA beam current with 30 second count times for each spot analysis. The instrument was calibrated prior to analyses using natural mineral standards.

Crystallographic preferred orientation (CPO) is a now routine data set that is used to study the crystallisation and deformation history undergone by geological samples. Importantly, CPO provides insight into the various processes and mechanisms by which samples crystallise and deform. Spatially resolved orientation data was obtained for olivine, clinoenstatite, magnetite, melilite and bytownite from automatically indexed electron backscatter diffraction patterns (EBSD) using the Zeiss EVO MA15 scanning electron microscope (with OXFORD Instruments Aztec Synergy EDS/EBSD software) at MQ Geoanalytical, in the Earth and Planetary Science (EPS) Department, Macquarie University, Sydney. The analyses were conducted with an accelerating voltage of 30 kV and working distance of 33 mm with a 70^{o} sample tilt under high vacuum. EBSD indexing was completed using the HKL CHANNEL 5 software. The HKL CHANNEL 5 software was used to process EBSD data. Noise reduction was achieved by replacing non-indexed solutions by the most common neighbour orientation. Grains were detected based on misorientation greater than 10^{o} and sub-grains detection is based on misorientation angles greater than 2^{o}. Grain orientation data was plotted on lower-hemisphere equal area projections and visualised using grain misorientation maps.

Results

Chondrule – alteration classification

Previous classification schemes (McSween, 1977; Gooding & Keil, 1981) did not discriminate between unaltered and altered chondrule. Whilst this is adequate to broadly classify and characterise chondrules across different chondrite groups, it fails to accurately describe chondrule populations within one chondrite. On this basis, a new scheme is developed to better document the textural and chemical evolution of chondrules in the solar nebular and in the chondrite parent-body. The modified classification scheme based on the Gooding & Keil (1981) and McSween (1977) scheme is firstly presented and summarised in Table 3.2. This scheme is only applicable to Type I chondrules as defined by McSween (1977). In the remainder of this contribution, we will use the proposed alternative scheme (Table 3.2). The classification scheme is summarised in Table 3.2.

Table 3.2 Summary of the classification scheme used in this study based on Gooding & Keil (1981) and McSween (1977) classification scheme.

Textural Classification			
Group	Primary crystallisation texture		
1	Barred olivine		
2	Porphyritic olivine		
Compositional Classification			
Type	Extent of nebula gas interaction	Subtype	Extent of parent body alteration
A	low (>80 vol% olivine)	1.0	no altered groundmass, no replacement of enstatite
AB	medium (intermediate modal adundances of olivine and pyroxene)	1.5	~50 % groundmass altered, ~50 % enstatite replaced
B	high (>80 vol% pyroxene)	2.0	> 95 % groundmass altered, >95 % enstatite replaced

Chondrule classification

Group 1 & 2: Group 1 and 2 represent crystallisation textures that are not exclusively restricted to the periphery of chondrules. Groundmass in group 1 and 2 chondrules is cryptocrystalline and anorthite in composition (Fig. 3.3a). In the chondrites surveyed, only barred olivine and porphyritic olivine of forsteritic olivine were found in this manner.

Type A, B & AB: The modification of group 1 and 2 textures by the pyroxene is approximated by Type A, AB, and B where A = >80 % olivine (Fig. 3.2a, b), B = >80 % pyroxene (Fig. 3.2d, e). Any intermediate compositions are classed as AB (Fig. 3.2c). Modification of the chondrule ground mass accompanying the increase in pyroxene abundance results in a change from glass to crystalline material (bytownite, augite and melilite) (Fig. 3.3, 2a and 2b).

Sub-type 1.0 – 2.0: The modification of previous classes by sodic and fayalitic olivine is recorded by the sub-type. Here, pyroxene is replaced by fine grains of fayalitic olivine and forsteritic olivine becomes increasingly Fe rich (Fig. 3.2c, f). Anorthitic groundmass is replaced by nepheline, sodalite and fayalitic olivine (Figure 3.3, 3a and 3b). A scale between 1.0 to 2.0 is presented based on the percentage area of alteration.

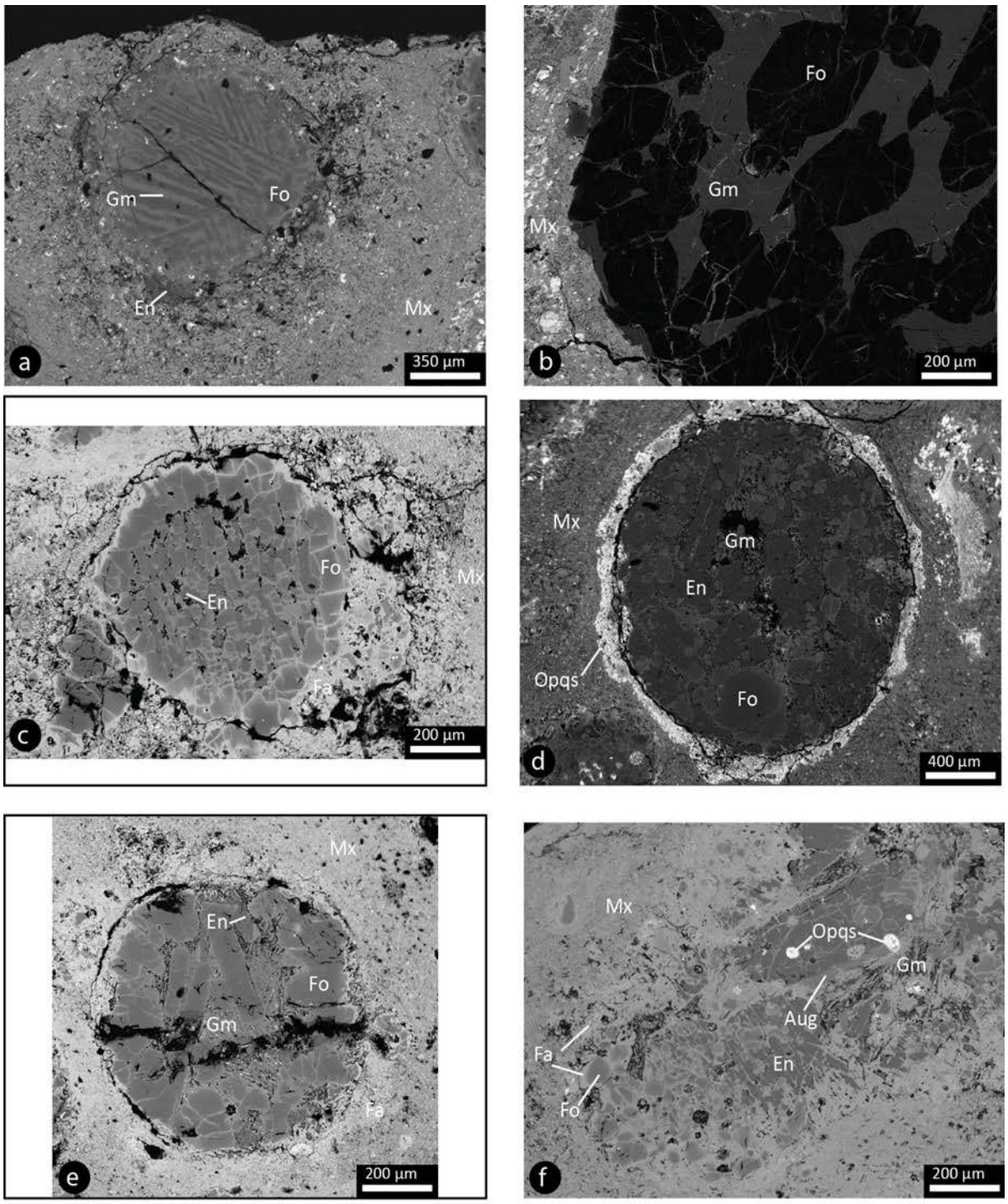

Figure 3.2 BSE image of a type IA 1.3 chondrule form Allende (a), enstatite at the edge is heavily replaced and minor amount of altered groundmass. Type IAB 1.5 chondrule (c), Ca-Al rich groundmass has altered to enstatite. Almost all of the rim has been replaced by fayalite rich olivine. Type IA 1.7 chondrule from NWA3118 (e), all the ground mass has been altered and ~70 % of the enstatite around the edge is replaced. Type IIA 1.0 chondrule from NWA4502 (b). Type IIB 1.1 chondrule from Allende (d). Type IIB 1.8 chondrule from NWA3118 (f) with extensive Fe zoning in olivine and heavy replacement of enstatite at the edge. Fo = forsteritic olivine, Fa = fayalitic olivine, En = enstatite, Aug = augite, Gm = chondrule groundmass, Mx = chondrite matrix, Opqs = magnetite + troilite.

Table 3.3 Representative compositions of phases in chondrules (wt%).

Phase	Chondrite	Occurrence	SiO2	TiO2	Al2O3	Cr2O3	FeO	MnO	MgO	CaO	Na2O	K2O	Cl	Total	Fo	Wo/An	En/Ab	Fs/Or
Ol	Allende	Pcryst core	43.03				2.92		54.05					100.00	97.0			
Ol	Allende	Pcryst rim	32.37	0.38	2.51	3.50	36.67		24.37	0.18				99.98	54.1			
Ol	Allende	Replacing Lpx	33.57		0.85		41.96		21.35	0.21				97.94	47.4			
Ol	NWA3118	Pcryst core	42.42				1.23		56.07	0.28				100.00	98.4			
Ol	NWA3118	Pcryst rim	33.94		5.68	0.65	29.89		29.69	0.80				100.65	63.1			
Ol	NWA3118	Replacing Lpx	35.91		0.26		34.69		29.14					100.00	60.0			
Ol	NWA4502	Pcryst core	42.40				1.59		54.93	0.60				99.52	97.7			
Ol	NWA4502	Pcryst rim	40.86				9.70		49.44					100.00	90.1			
Ol	NWA4502	Replacing Lpx	36.19				34.52		29.29					100.00	60.2			
Lpx	Allende	Pcryst core	59.95		0.37	0.60	3.76	0.23	37.01	0.22				102.14		0.4	94.2	5.4
Lpx	Allende	Pcryst rim	57.65	0.15	1.66	1.68	5.41	0.81	31.86	2.76				101.98		5.4	86.4	8.2
Lpx	NWA3118	Pcryst core	56.46		1.59	0.57	2.90		36.42	0.69				98.63		1.3	94.5	4.2
Lpx	NWA4502	Pcryst core	59.02		0.54	0.57	0.67		38.82					99.62		0.0	99.0	1.0
Hpx	Allende	Pcryst rim	51.67	0.49	6.10	2.87	4.42	0.79	19.39	15.34				101.07		33.5	59.0	7.5
Hpx	NWA3118	Pcyrst rim	53.58	0.70	3.53	1.01	0.85	0.60	21.24	18.49				100.00		37.6	60.1	2.3
Hpx	NWA4502	Pcryst rim	53.36	1.34	3.36	0.46			20.80	20.68				100.00		41.7	58.3	0.0
Plg	Allende	fine-grain in ground mass	47.07		32.57		0.95			17.01	1.77			99.37		84.2	15.4	
Plg	NWA3118	fine-grain in ground mass	46.45		32.74		1.33			17.35	1.75			99.62		84.6	15.4	
Sod	NWA3118	fine-grain in ground mass	36.99		31.61		0.30				23.78		7.22	99.90				
Nep	Allende	fine-grain in ground mass	39.23		35.98		1.51			0.63	18.90			96.25				
Nep	NWA3118	fine-grain in ground mass	42.73		35.74		0.53			2.57	16.23	2.11		99.91				
Gm	Allende	groundmass	47.07		32.57		0.95		0.62	17.01	1.77			99.99				
Gm	NWA4502	groundmass	43.89	2.33	15.78	0.36	0.61		12.38	24.64				99.99				
Agm	NWA4502	groundmass	47.67	0.97	22.71		3.53		5.66	8.46	10.12	0.88		100.00				

Pcryst: phenocryst, Ol: olivine, Lpx: low Ca pyroxene, Hpx: high Ca pyroxene, Plg: plagioclase, Sod: sodalite, Nep: nepheline, Gm: cryptocrystalline groundmass, Agm: Altered groundmass.

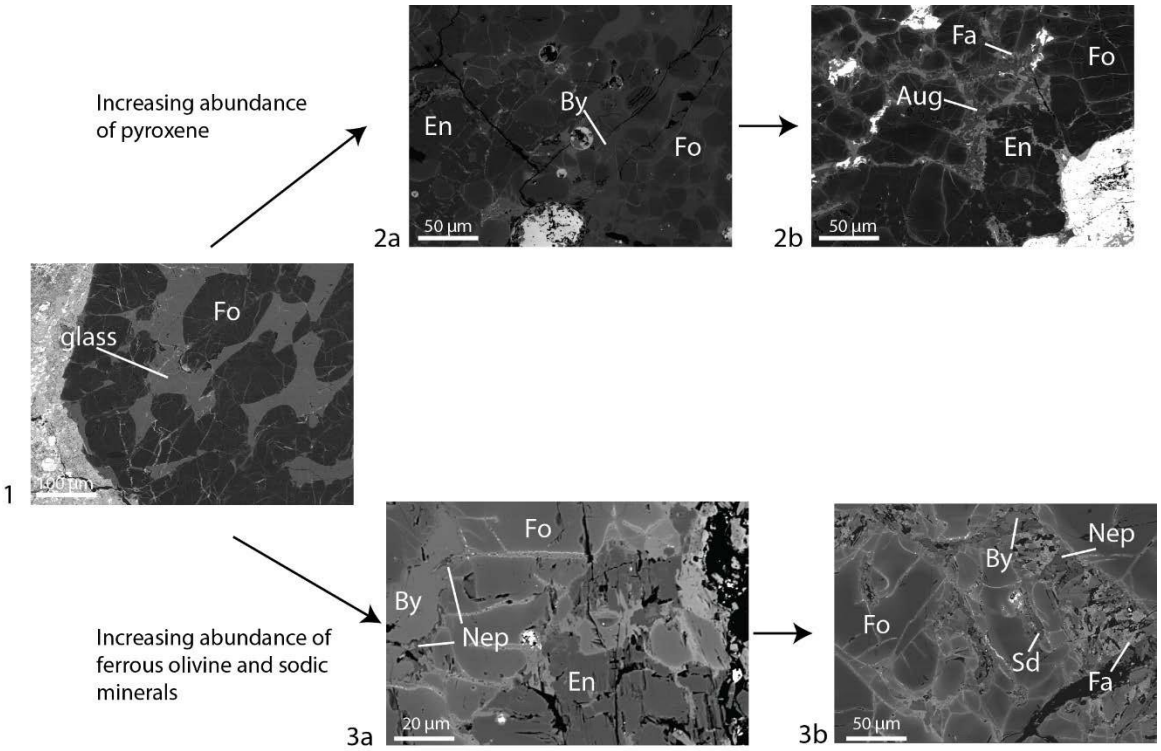

Figure 3.3 Unmodified chondrule glass (1). Modification of chondrule with increasing abundance of pyroxene (2a and 2b) and with increasing fayalite, nepheline and sodalite (3a and 3b).

Mineral chemistry: Overview

Three occurrences of olivine are observed within the studied chondrules. These include; i) phenocrysts, ii) fine-grains set in the chondrule groundmass and iii) fine-grains replacing Low-Ca pyroxene. Olivine phenocrysts are consistently Fo rich ($Fo_{>95}$) in unaltered chondrules with increasing fayalite component in altered chondrule. Olivine phenocrysts in NWA3118 and Allende are often chemically zoned with Fe increasing toward the grain boundaries and along fractures with typical compositions between Fo_{50-65} (Fig 3.4a). In addition to Fe increasing, these areas often mark the appearance of Al_2O_3 and CrO (Table 3.3). Olivine found as fine grains in the chondrule groundmass and replacing Low-Ca pyroxenes are consistently Fa rich with compositions ranging between Fo_{45-60}. Chondrules which contain CaO in olivine display a step function with a general trend of decreasing CaO with increasing FeO (Fig. 3.4b). In chondrules containing no CaO in forsteritic olivine cores, CaO can be found in the rim and along grain boundaries < 1.0 wt. %.

Based on Wo and En end member compositions, pyroxene analyses class as either enstatite or augite (Fig. 3.4c). One analysis was classified as the high temperature variant pigeonite. Minor element composition of enstatite (Al_2O_3, TiO, CaO, Cr_2O_3) varies by 1-2 wt. % between individual chondrules. Augite is observed predominately as rims around enstatite phenocrysts and as fine grains in the chondrule groundmass. Minor element composition of augite

from the same chondrule is consistent and Al_2O_3, TiO_2, CaO and Cr_2O_3 are always greater in augite compared to enstatite within the same chondrule.

Plagioclase and nepheline are found exclusively as fine grains within the chondrule groundmass, the abundance of nepheline reflects the intensity of parent body alteration (Fig. 3.2 3a and 3b). All plagioclase analyses from Allende and NWA3118 classify as bytownite with an enriched An component (An_{85}). Minor element compositions are consistent across both chondrites and variation within 1% occurs between different chondrules. K_2O content is found to be consistently low, below detection limit in all plagioclases analysed. Nepheline contains 0.4-2.8 wt% CaO and up to 2.6 wt% K_2O. Sodalite was only analysed in NWA3118 (Fig. 3.2, 3b).

Cryptocrystalline chondrules groundmass is mainly observed in the less altered chondrules of NWA4502 (Fig. 3.2). Pristine chondrule ground mass has near pure anorthite composition, NaO, K_2O and MnO are all below detection limit. Altered chondrule ground mass in chondrules from NWA4502 (Table 3.3) relatively decrease in CaO and MgO. Altered groundmass also marks the appearance of NaO and K_2O. Variability in FeO, CrO and TiO in altered chondrule ground mass is within the variation of pristine groundmass between different chondrules.

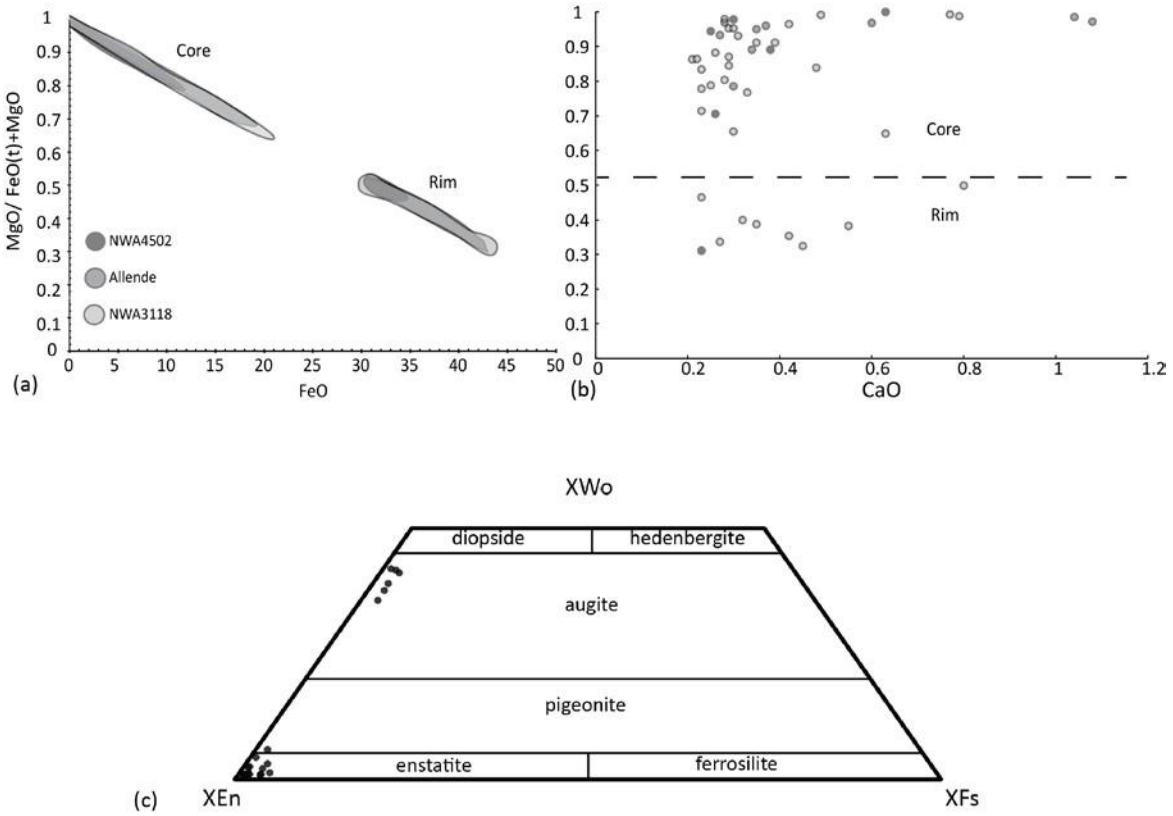

Figure 3.4 Plots showing the correlation between MgO/FeO(t)+MgO with FeO (a) and CaO (b). Pyroxene classification diagram (c) shows that the majority of pyroxene class as either augite or enstatite. One analysis of an enstatite rim was classified as pigeonite.

Chondrule microstructures

Allende-003 is classed as a group 2B 1.1 chondrule and composed of clinoenstatite (En_{94}, Fs_4) and olivine phenocrysts ($Fo_{>95}$) with ground mass containing augite (En_{34}, Wo_{60}), fayalitic olivine ($Fo_{<60}$) and sodic melilite (Fig. 3.5a and 3.5d). Magnetite and troilite is absent in the interior and form a continuous rim around the chondrule (Fig. 3.5a). Clinoenstatite phenocrysts are euhedral and tabular, grain sizes vary from 100 µm to 300 µm. Augite is found as 3µm – 10µm thick discontinuous rims on clinoenstatite grains or as fine grains in the chondrule groundmass. Clinoenstatite grain boundaries in contact with the chondrule groundmass record local misorientation angles of ~3^o (Fig. 3.5c). Similar misorientation angles are seen in Ca-Al rich fractures (Fig. 3.5d). Clinoenstatite twinning extends into the ground mass, preserved by melilite and augite. Forsteritic olivine phenocrysts are poikilitically enclosed by clinoenstatite and exhibit embayed grain boundaries. Grain boundaries and fracture in olivine phenocrysts are enriched in Cr and Fe relative to the phenocryst interior. Misorientation angles within olivine phenocrysts are below 1^o. Olivine phenocrysts can preserve well develop facets when in contact with the chondrule groundmass (Figure 3.4d).

Allende-001 is a group IA 1.4 chondrule, containing multiple sets of parallel olivine platelets ($Fo_{>95}$) enclosed by a continuous olivine shell ($Fo_{>90}$) (Fig. 3.6a, b). Clinoenstatite (En_{94}) is observed at the edge of the chondrule and in the chondrule groundmass (Fig. 3.6b). The olivine shell is embayed by clinoenstatite on the outside edge and olivine platelets are embayed where clinoenstatite is crystallised in the groundmass (Fig. 3.6b, e). Parallel sets of olivine platelets and attached olivine shell have the same orientation and grain orientations vary between different sets (Fig. 3.6c, d). Orientation data for olivine is tightly clustered (Fig. 3.6c). One section of the olivine shell contained sub-grain boundaries forming perpendicular to the edge of the chondrule. Clinoenstatite around the edge of the chondrule displays well developed multiple twinning and is mostly replaced by fayalitic ($Fo_{<60}$) olivine (Fig. 3.4d). Clinoenstatite in the chondrule ground mass contain multiple twinning; however twinning is less developed (Fig. 3.7a). The chondrule ground mass is predominately bytownite which are either rounded or elongate when restricted by small spacing of olivine bars (Fig.3.5d, e). Bytownite orientations show a close relationship to the orientation of the barred olivine (Fig. 3.7c, e).

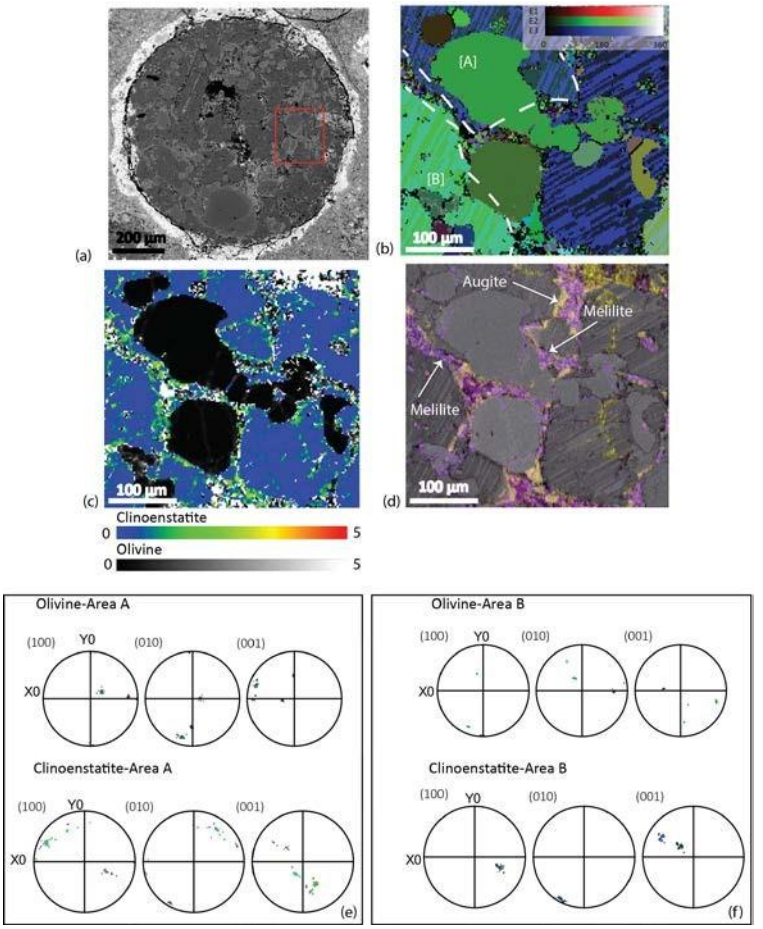

Figure 3.5 Characteristics of a Group 2B 1.1 chondrule, Allende-003 (a) with Euler map (b) showing the orientation of each grain with respect to the three Euler angles (site map is highlighted in the red box). Texture component map (c) showing local misorientation angles in olivine and clinoenstatite. Chemical map of the site (d) showing the distribution of Ca (yellow), Na (blue), Al (pink) and Fe (red). Grain orientation of olivine compared to clinoenstatite in area A and B (e) and (f) respectively.

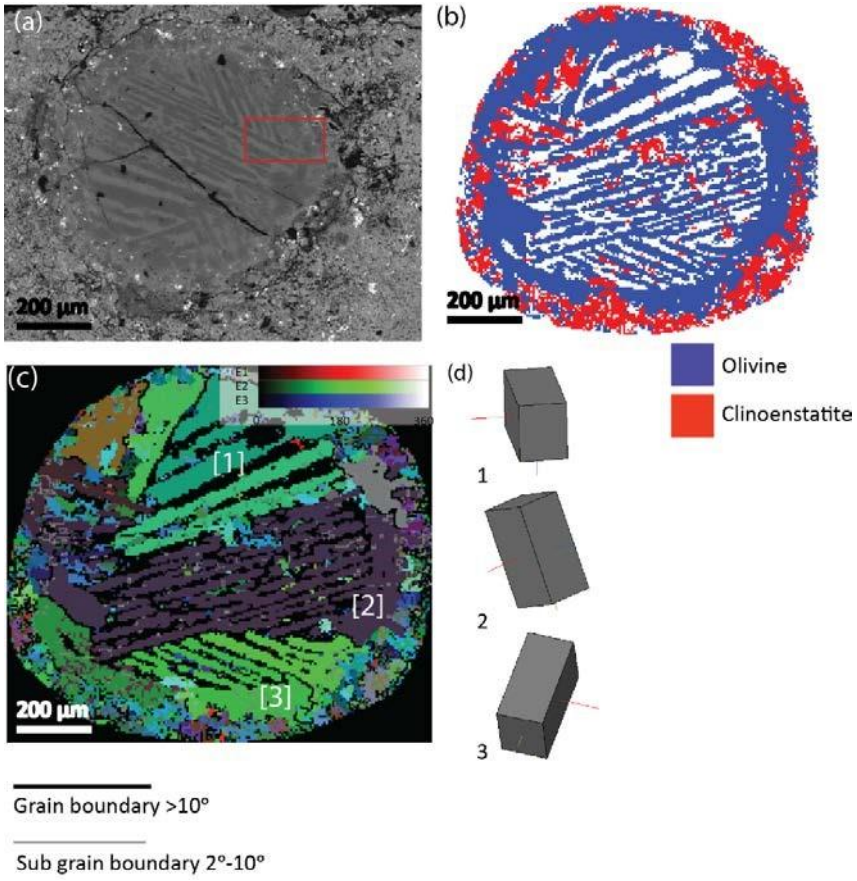

Figure 3.6 Characteristics of a group 1A 1.4 chondrule (a) with phase map (b). Overview Euler map highlighting the orientation of olivine bars (c) with 3D representation of orientation visualised (d).

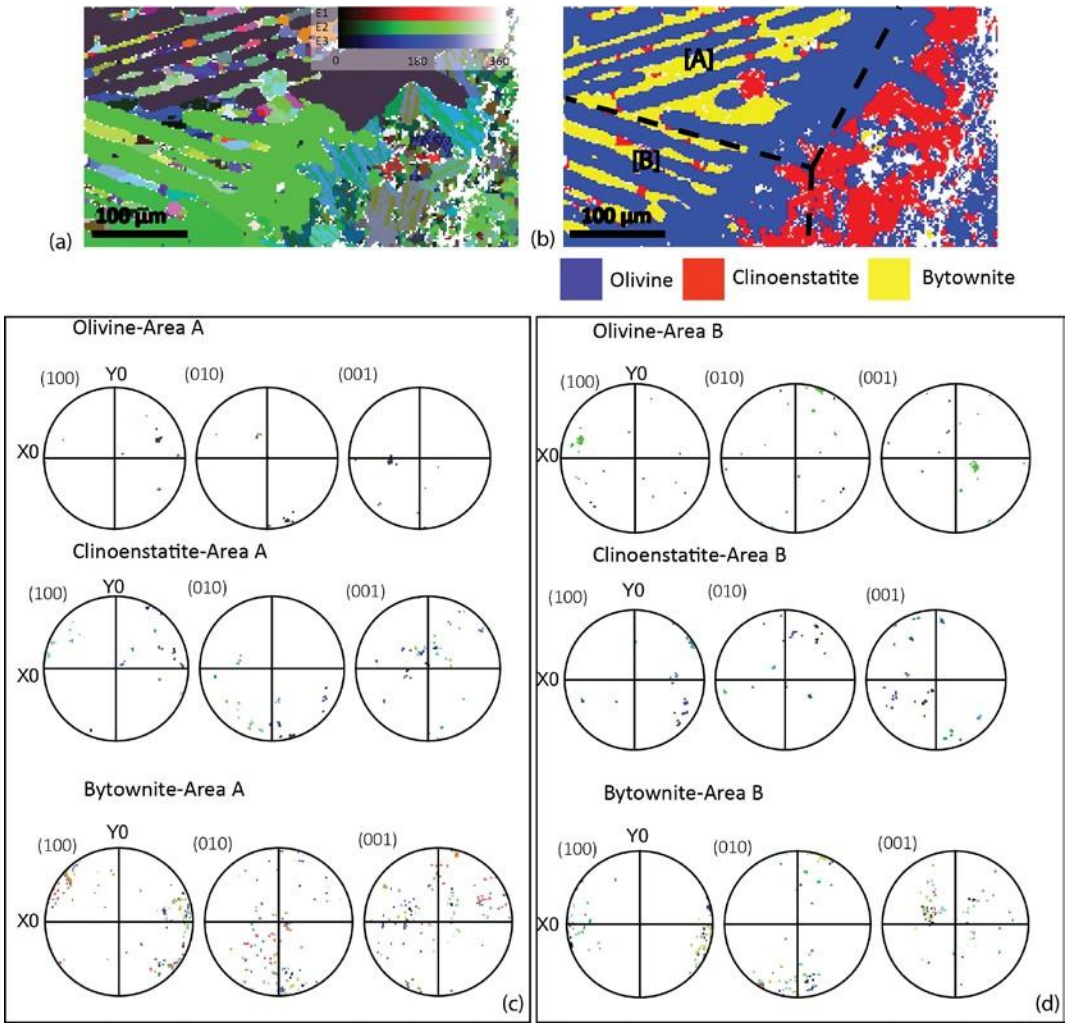

Figure 3.7 Euler map highlighting the orientation of olivine, bytownite and clinoenstatite (a) (area highlighted with a red rectangle in Fig. 3.6) and phase map (b). Olivine, clinoenstatite and bytownite data are presented on lower hemisphere equal area projections for area A and B (c) and (d) respectively.

Chondrule NWA3118-001 is a group IAB 1.6 chondrule and contains one parallel set of olivine platelets ($Fo_{>90}$) encompassed by a continuous, olivine shell ($Fo_{>85}$) (Fig. 3.8a). Although the platelets are all parallel, the chondrule is made up of at least four grains based on the orientation of olivine (Fig. 3.8c, d). The olivine shell contains sub grain boundaries forming perpendicular to the edge of the chondrule (Fig. 3.8c). The shell olivine is embayed on the outside where remnant clinoenstatite is present (Fig. 3.8a, b). The chondrule groundmass is made up entirely of clinoenstatite (En95, Fs4) with minor clinoenstatite found at the edge. Clinoenstatite in the chondrule groundmass can contain well developed twins depending on the grain size (Fig. 3.8c) Clinoenstatite and olivine grains share similar crystallographic orientations, this is most visible in the (010) and (001) planes (Fig. 3.8e and f).

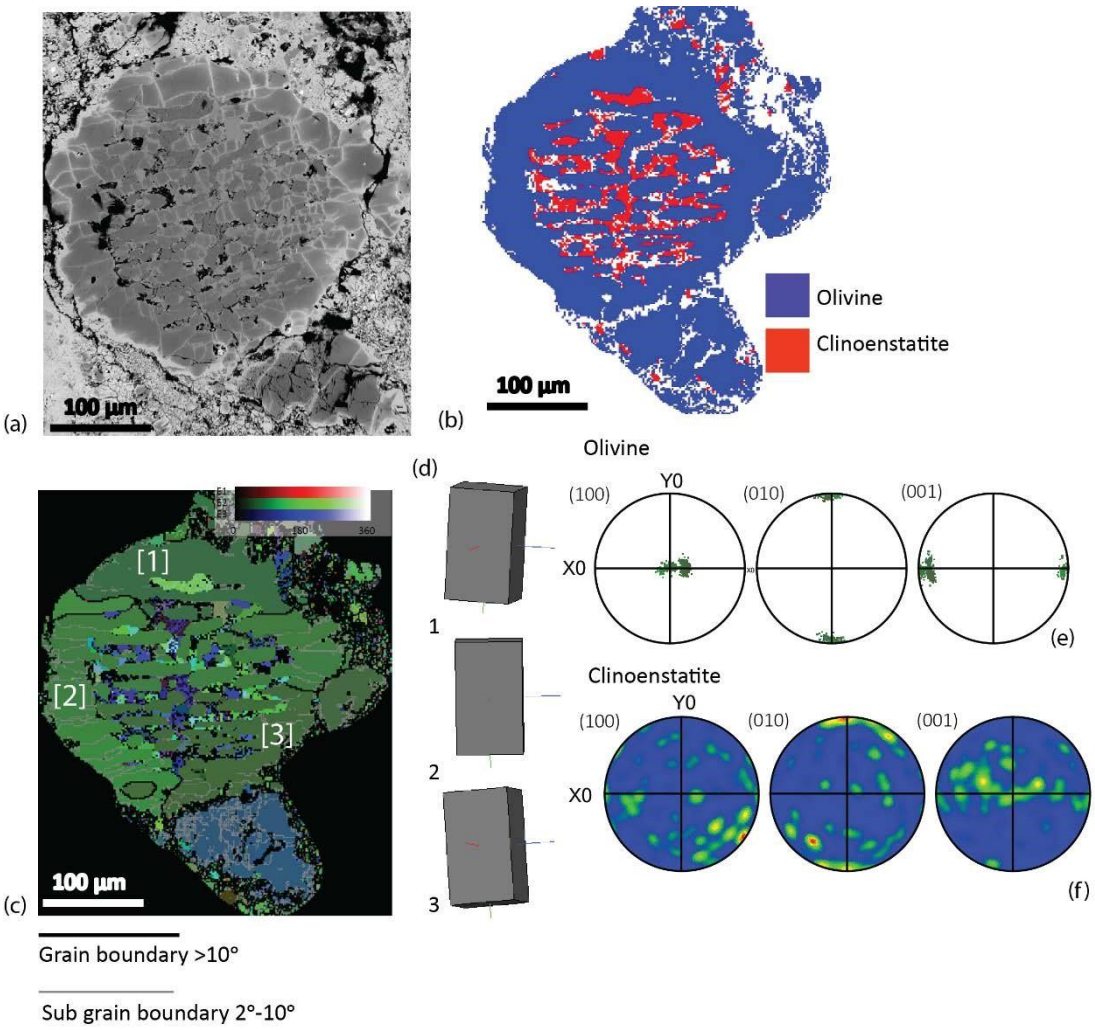

Figure 3.8 Characteristics of a group 1A 1.5 chondrule, NWA3118-001 (a) with phase map (b) showing olivine and clinoenstatite. Euler map (c) with grain (black) and sub grain boundaries (grey) for olivine. Clinoenstatite orientations plotted on a lower hemisphere, equal area projection showing preferred orientation most visible in the (010) and (001) plane (f).

Allende-002 is a group 2A 1.6 chondrule, it is predominately composed of equigranular olivine (Fo>90) set in a cryptocrystalline chondrule groundmass (Fig. 3.9a). Magnetite and Fe, Ni sulphides are present as amorphous pools interstitial to olivine phenocrysts (Fig. 3.9 a). Olivine grains exhibit random orientations (Fig. 3.9 6b) and well-developed crystal facets when not in contact with other grains (Fig. 3.9d). Misorientation angles within the interior of olivine grains are less than 1^{o} (Fig. 3.9). Olivine in the alteration zone display up to 2^{o} misorientation in the outer 5 µm – 10 µm section of the grain and less than 1^{o} misorientation in the interior (Fig. 3.10). In comparison, olivine in the unaltered zone exhibit misorientation angles less than 1^{o} in the interior and toward to the grain boundary. Chondrule groundmass is non-crystalline and anorthite in composition in the unaltered core. Alteration of the groundmass results in a loss of Ca and Al reflecting a change in mineralogy from anorthite composition glass to Fe-rich olivine (Fig. 3.9b). Ca rich spots can be seen in the periphery of the chondrule (Fig. 3.9b).

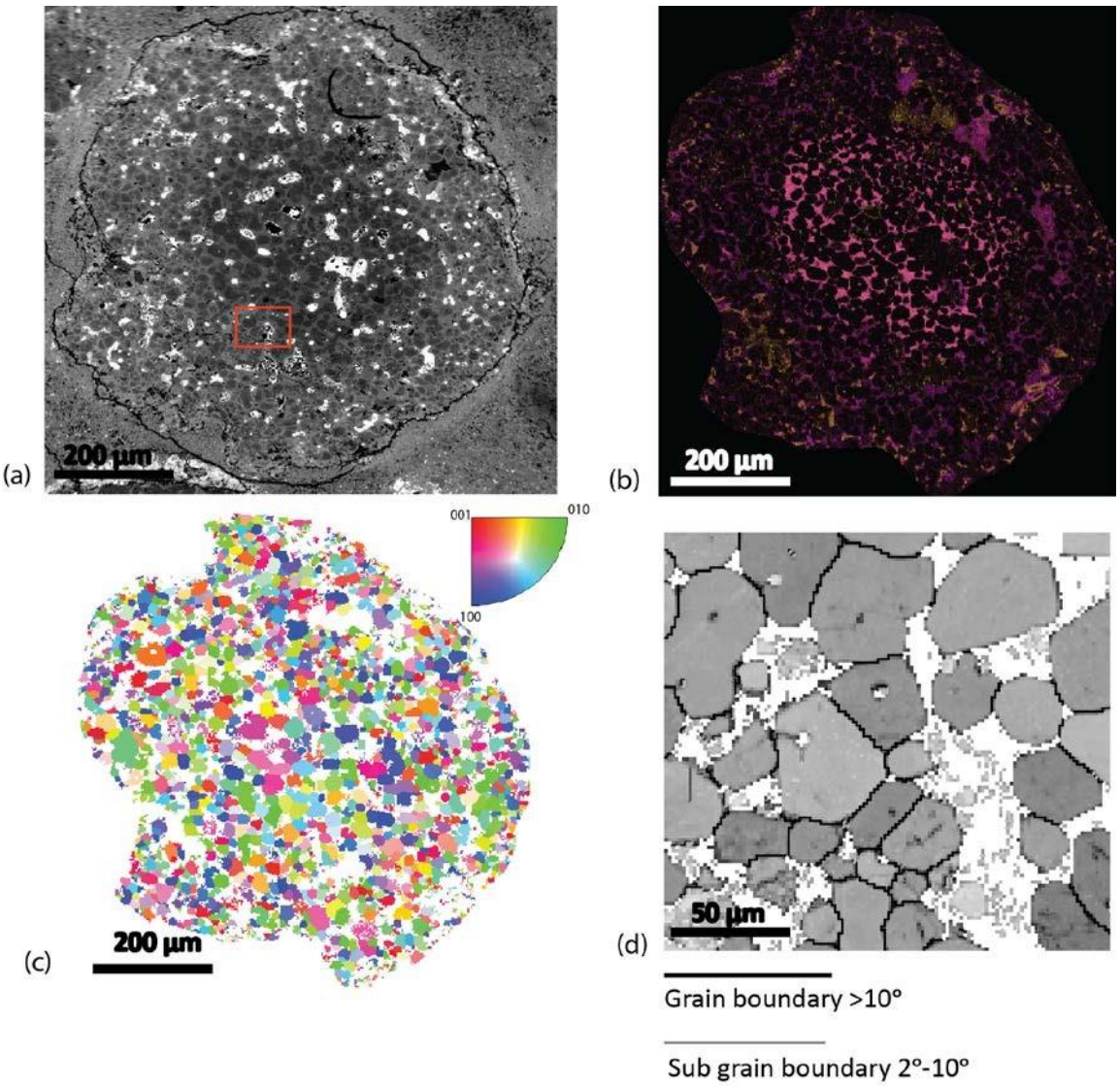

Figure 3.9 BSE image overview of Allende-002 (a) and overview IPF map showing the orientation of olivine grains (c). Element map comparing the abundance of Al (pink) and Ca (yellow) in the altered rim and unaltered core (d). Ca rich areas can be found along the edge of the chondrule. Band contrast, close up of the region shown in the red box (d) showing no sub-grain boundaries and well developed crystal facets in olivine.

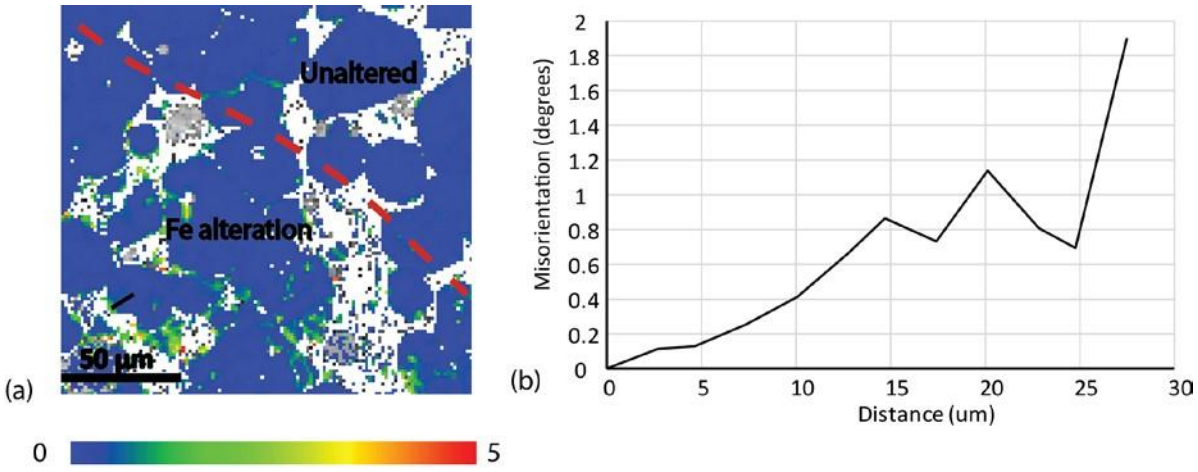

Figure 3.10 Map of the texture component for Allende-002 (a) (map area highlighted in the red box in Figure 3.6a). Misorientation profile (red transect line) showing an increase in the misorientation angle in the outer 5 µm of the grain.

Discussion

Chondrule classification: measuring nebular and parent-body interaction

Dynamic crystallisation of an olivine rich melt has been shown experimentally to replicate porphyritic and barred olivine textures (Lofgren & Russel, 1986; Lofgren & Lanier, 1990). On this basis, Group 1 and 2 are interpreted to represent a primary crystallisation texture. Porphyritic pyroxene textures were also reproduced this way (Lofgren & Russel, 1986). However, pyroxene is always zoned toward the edge of chondrules and chondrule groundmass is always crystalline in the presence of pyroxene. Previous studies have demonstrated that the abundance of pyroxene in is the result of chondrule-melt interaction with silica rich gas in the nebular (Tissander et al., 2002; Libourel et al. 2006; Marrocchi & Libourel, 2013). A and B types can be used to approximate the measure of nebular gas interaction experience by a given chondrule. Fayalitic olivine, nepheline and sodalite are always observed to overprint type A, B modification. Therefore, subtype 1.0-2.0 describes the extent of parent body alteration and is determined by the extent of groundmass alteration, enstatite replacement by fayalitic olivine, Fe rich zoning in olivine (Kimura & Ikeda. 1995).

Nature of chondrule alteration: The results of Nebular gas – chondrule interaction

The formation of Low-Ca pyroxene rims around olivine chondrules is widely recognised as the primary mineral associated with gas-melt interaction (Tissander et al., 2002; Libourel et al. 2006). EBSD analyses has revealed that this previously described phase is clinoenstatite in all three chondrites studied (Fig. 3.5, 3.6, 3.7, 3.8). Experimental studies of the polymorphism of enstatite have shown that clinoenstatite forms when cooling rates are sufficiently high enough (Smyth, 1974). Under these conditions, protoenstatite inverts to polysynthetically twinned clinoenstatite or to a mixture of clinoenstatite and orthoenstatite (Foster, 1951; Smyth, 1974). Clinoenstatite can also form by mechanical deformation (Turner et al., 1960) however this type of transition is typically localised in kinks and does not display twinning (Boland, 1975; Coe & Kirby, 1974). All Low-Ca pyroxene are observed as the clinoenstatite polymorph and most chondrule have experienced little mechanical deformation. The formation of clinoenstatite is attributed to fast cooling rates rather than deformation. High cooling rates required to form clinoenstatite is consistent with dynamic crystallisation experiments of chondrules melts which predict cooling rates in the order of 100^{o}C/hour (Lofgren, 1988).

Clinoenstatite is found to enclose olivine or corrode olivine grain boundaries indicating that olivine had already crystallised. In barred olivine chondrules, clinoenstatite is observed crystallising along grain boundaries of olivine bars. Clinoenstatite found at the edge of chondrules and in the chondrule groundmass are chemically and texturally similar, strongly suggesting that both are genetically related. For the minor element composition, variation in the order of 1 – 5 wt. % is observed between different chondrules within the same chondrites rather than a systematic variation across the three chondrites

Nebular gas interaction is likely responsible for the first generation of Fe-zoning in chondrule olivine. Olivine enclosed by clinoenstatite often exhibit Fe enrichment along the grain boundary, this is also observed in chondrule Allende-003 (Fig. 3.5a). In Allende-003 there was no correlation between Fe-enrichment along the grain boundary and increase in the misorientation (Fig. 3.5c). In comparison olivine in Allende-002 demonstrated an increase in the misorientation angle along grain boundaries in contact with the Fe-rich altered groundmass (Fig. 3.7). Fe zoning in olivine produced during nebular gas interaction with chondrule melt is driven by simple diffusion and does not result in a textural change.

Mineral composition of olivine and enstatite indicates that Si was the main element introduced into the system. In this interpretation, the formation of clinoenstatite occurred by the following reaction (Tissandiar et al., 2002);

$$\text{Olivine} + \text{melt}_1 + \text{Si}_{(g)} = \text{Orthopyroxene} + \text{melt}_2$$

The Allende-003 chondrule is unique in that the sulphide rim has prevented significant parent body alteration as evident by the preservation of clinoenstatite. Therefore, nebular gas interaction is better preserved. The chondrule groundmass is composed of augite at the edge and melilite in the centre (Fig. 3.5d). Local misorientation angles of 3^{o} are found along clinoenstatite grain boundaries and fractures. Spruzeniece et al. (2016) found that 'deformation' like textures were produced during fluid mediated dissolution-precipitation reactions. The observation of these textures only along grain boundaries and not in the grain interior strongly suggests they are alteration related. Evidence for replacement of clinoenstatite is also found by melilite replicating twin planes (Fig. 3.5d). The interaction between groundmass and clinoenstatite is one of alteration and not crystallisation. On this basis, an alternate model of nebular gas-chondrule interaction is presented where Si rich gas interacts with an already crystallised chondrule. In this model, the mineralogy observed in Allende-003 is produced by the following reactions;

$$\text{Olivine} + Si_{(g)} = \text{Orthopyroxene}$$

$$Glass_{(An)} + Si_{(g)} = \text{Melilite} + \text{Clinopyroxene}$$

If nebular gas interaction occurred in this way, then the recrystallization of chondrule glass also occurred during this interaction. Chondrules that have no clinoenstatite or minor clinoenstatite around the periphery preserve a glassy groundmass (Fig. 3.2b). In chondrules with notable clinoenstatite at the edge, the groundmass crystallised to bytownite (Fig. 3.5e). During interaction with hot nebular gas, heat is transmitted through the chondrule causing the chondrule glass to crystallise. The orientation of bytownite and clinoenstatite is correlated with the orientation of olivine bars (Fig. 3.7 and 3.8). This relationship is interpreted to represent nucleation occurring on the grain boundary of the olivine bars, for clinoenstatite this is clearly visible (Fig. 3.7b). The chondrule size is negligible for the transfer of heat, but the chemical change lags behind i.e. the formation of clinoenstatite at the rim.

Nature of chondrule alteration: Parent-body alteration

Parent body alteration has resulted in secondary minerals identified in this study including; nepheline, melilite, sodalite and Fe-rich olivine. Fe-rich olivine (Fo_{45-60}) is found in the chondrule ground mass, in fractures within forsteritic olivine grains, replacing clinoenstatite and replacing magnetite. Fe enrichment (Fo_{55-65}) along grain boundaries of forsteritic olivine grains is also attributed to parent body alteration. The appearance of Al_2O_3 in the Fe-enriched rim of up to 4 wt.% appears to be characteristic of this Fe zonation. In comparison, Fe zonation interpreted as having formed during gas interaction does not display this correlation with Al_2O_3. Olivine replacing clinoenstatite always have less Al_2O_3 compared to the Fe-rich rims. Partly altered group 2 chondrules (Fig. 3.6) exhibit a reduction in olivine grain sized compared to the unaltered cores. The outer 5-10 um of olivine grains in the altered section show an increase of local misorientation from less than 1^o in the core up to 3.6^o at the rim. In comparison, Fe-rich zoning that occurred in the nebular does not show a change in local misorientation from the core to the rim. As such, Fe enrichment during parent-body alteration does not occur only by simple diffusion.

The formation of sodic minerals occurs as a replacement reaction with amorphous or crystallised chondrule groundmass of anorthite/bytownite compositions. A summary of the reaction is based on element maps and mineralogy of primary and secondary minerals is as follows; Na, K, Fe and Cl was introduced into chondrules, Ca and Si was removed or redistributed.

In a study of CV chondrites, Ikeda & Kimura (1997) proposed that nepheline and sodalite formed at temperatures less than 800 K by gas-solid reactions in the solar nebula. The relative abundance of alteration intensities observed in individual chondrules is not uniform across each chondrite, with a clear progression of alteration intensity observed across the three chondrites. If this alteration occurred as a nebular process, then it should result in a more uniform distribution seen in the type A, AB and B chondrules. This evidence implicates parent-body alteration in the formation of secondary sodic mineral in support of Bischoff's et al. (1988) and Tomeoka's (1997) conclusion. Furthermore, previous studies have found secondary minerals in all the chondritic components (chondrules, refractory inclusions and matrix) in CVAxO chondrites (MacPherson et al., 1988; Krot et al., 1995) providing additional evidence for this alteration occurring on the parent-body.

Although the location of the sodic and Fe-rich olivine secondary mineralisation on the chondrite parent body is well constrained, the relative timing of these mineralisation events is ambiguous. Kimura & Ikeda (1995) noted that whether the nepheline and sodalite replacement reaction occurred pre, contemporaneously or post formation of ferrous olivine and Fe-rich zoning was unclear. In this study we find that the amount of altered groundmass is related to the extent of Fe-rich olivine formation and extent of Fe zoning in forsteritic olivine. This is best demonstrated in the progression of alteration intensity observed between the three sampled chondrites. Though not an explicit link, it does support contemporaneous formation for both nepheline + sodalite and fayalitic olivine secondary mineralisation. The change of magnetite to Fe-rich olivine requires the addition of Si. Assuming the original composition of the groundmass is anorthite, the reaction to form nepheline results in the liberation of Si. Although Si could have also been introduced externally by fluids, release of Si by reacting anorthite to form nepheline is consistent with the observation of Fe-rich olivine replacing magnetite.

Model for CV_{oxA} history: messengers from outer space

Although all chondrules in NWA3118 and Allende along with most in NWA4502 exhibit the same style of alteration, the extent of alteration varies within each chondrite. NWA3118 contained the highest percentage of highly altered chondrules. Chondrules in NWA4502 experienced very little parent-body alteration. In comparison, the relative abundance of type A, AB and B chondrules as measured by the abundance of clinoenstatite are consistent between NWA3118 and Allende (Figure 3.11). NWA4502 contained more B and AB chondrules. Since clinoenstatite is readily replaced by fayalitic olivine during parent-body alteration, type B and AB chondrules are

less likely to be preserved during parent body alteration. This is best demonstrated in the NWA3118 chondrite in which some type B chondrules are almost entirely altered to fayalitic olivine (Figure 3.3f). Gooding & Keil (1981) observed that the relative abundance of different chondrule types in ordinary chondrites were all similar. This implies that the chondrule population from each chondrite samples the same nebular source region. As noted by (Gooding & Keil, 1981), the uniformity in relative abundances of chondrule types also indicates that regions of chondrule formations are well homogenised before material aggregates to form the chondrite parent body. Although not conclusive, the distribution of a feature in chondrules could be used to provide evidence for nebular or parent body process. For example, the relative percentage of altered chondrules between the CV chondrites studied does not show uniform a distribution between the samples and therefore the distribution of altered chondrules is better explained by localised alteration on the parent body.

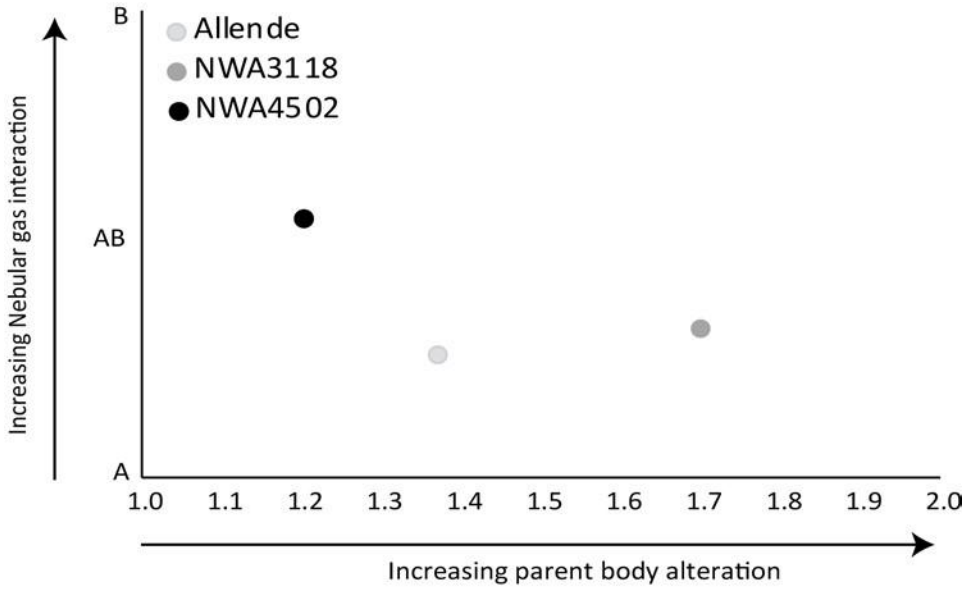

Figure 3.11 Plot of the average chondrule type (A. AB, B) and average extent of parent body alteration

One important constraint on the formation of the final lithology is whether alteration occurred in-situ or in different source regions. The chondrule population from each chondrite shows an average increase in the relative abundance in alteration intensity of individual chondrules from NWA4502 to NWA3118. However, each chondrite contains chondrules which exhibit a range of alteration intensities. In NWA4502 this range is relatively small from 1.0 to 1.3 whilst Allende and NWA3118 show a much higher range of alteration intensities. This initially suggests that the little parent body alteration experienced on NWA4502 was in-situ. In the case of Allende and NWA3118, the wide range of alteration intensities may require multiple source

regions. Previous studies of Allende have identified dark inclusions in Allende, clasts which contain similarly altered chondrules and matrix but generally to a greater extent (Fruland et al., 1978; Kurat et al., 1989; Kojima & Tomeoka et al., 1996; Krot et al., 2001). These points toward multiple sources on the chondrite parent body. This process transitions away from a simple direct accretion of solar nebular materials (Wood, 1963, 1985; Metzler et al., 1992) to a more dynamic model of fragmentation of material in different source regions followed by transportation and deposition (Tomeoka & Ohnishi, 2015).

Conclusion

Chemical and structural analysis of chondrules from three CV_{oxA} chondrites in this study has revealed the following;

1. The three chondrites studied form a progression in parent-body alteration intensity, from the relatively pristine NWA4502 chondrite to the extensively altered NWA3118 chondrite.
2. Chondrules formed in a similar environment based on mineral chemistry, individual chondrules contain small variation in minor elements 1 – 5 wt %. Distribution of type A, AB and B chondrules in each chondrite is roughly the same indicating chondrule population from each chondrite is similar.
3. The range of alteration intensities observed in individual chondrites provides evidence for alteration in the CV chondrite occurring in different regions. The final lithology is thus formed by fragmentation, transport, and deposition of chondrules from different source regions on the chondrite parent-body.
4. The correlation between the extent of Fe-rich olivine zoning and mineralisation and the abundance of altered groundmass gives evidence for contemporaneous mineralisation.

Chapter 4: Thesis conclusion

Visualisation and quantification of CM and CV components demonstrate that the chondrite lithology is formed by mixing material from different source regions. A new chondrule classification scheme is presented and used to demonstrate variability in the extent of parent body alteration in the chondrule populations of NWA3118, Allende and NWA4502. On this basis, chondrules can be viewed as 'sediments' from different source regions on the chondrite parent-body. CM chondrites are characterised by high modal abundance of matrix. In the CV chondrites, the modal abundance of matrix is associated with alteration. These relationships are best explained if chondrite meteorites formed in a dynamic environment. In the model presented in Chapter 2, the CM and CV chondrite lithology both form by fragmentation, transport and agglomeration. The difference between the two types of chondrites is the temperature of the environment in which they were altered i.e. high temperature for CV and low temperature for CM.

Chondrule groundmass is found to be crystalline in the presence of peripheral pyroxene. In chondrules where no pyroxene is present and parent-body alteration is absent, the groundmass is glassy. Evidence of dissolution-precipitation reactions is found in pyroxene grain boundaries in contact with matrix. These relationships between pyroxene and chondrule ground mass is easily explained if hot Si rich nebular gas interacts with an already cooled chondrule. Heat is transferred uniformly in the chondrules causing recrystallization of glass. The chemical change has progresses slower and results in the formation of pyroxene in the periphery.

Suggestions for further studies

Considering the context of chondrite meteorites, the role of impacts in the producing the chondrite lithology is emphasised. It is plausible that each stage of fragmentation, alteration, transport and lithification is mediated by impacts. This requires two lines of investigation. Firstly, EBSD analysis of the meteorite matrix should be conducted on samples representing a progression of alteration to determine any correlation between alteration and shock stage. High pressure minerals formed during impacts may be preserved in the matrix and finding these may provide a crucial link. Secondly, granular flows in low gravity environments and aeolian transport during transient atmosphere can be investigated by numerical modeling to better evaluate these processes as a viable mechanism to smooth and transport particles on the chondrite parent body.

References cited

Alexander, C.O.D., Grossman, J.N., Ebel, D.S. and Ciesla, F.J., 2008. The formation conditions of chondrules and chondrites. *Science*, *320*(5883), pp.1617-1619.

Anders, E. and Grevesse, N., 1989. Abundances of the elements: Meteoritic and solar. *Geochimica et Cosmochimica acta*, *53*(1), pp.197-214.

Baker, L., Franchi, I.A., Wright, I.P. and Pillinger, C.T., 2002. The oxygen isotopic composition of water from Tagish Lake: Its relationship to low-temperature phases and to other carbonaceous chondrites. *Meteoritics & Planetary Science*, *37*(7), pp.977-985.

Bouvier, A., Wadhwa, M., 2010, The age of the Solar System redefined by the oldest Pb-Pb age of a meteoritic inclusion, nature geoscience, vol. 3, pp.637-641.

Buseck, P., Hua, X., 1993, Matrices of carbonaceous chondrite meteorites, Annual Reviews of Earth and Planetary Sciences, vol. 21, pp.255-305.

Boss, A.P. and Durisen, R.H., 2005. Chondrule-forming shock fronts in the solar nebula: A possible unified scenario for planet and chondrite formation.*The Astrophysical Journal Letters*, *621*(2), p.L137.

Brearley, A.J. and Krot, A.N., 2013. Metasomatism in the early solar system: The record from chondritic meteorites. In *Metasomatism and the chemical transformation of rock* (pp. 659-789). Springer Berlin Heidelberg.

Carlson, W.D., 2006. Three-dimensional imaging of earth and planetary materials. *Earth and Planetary Science Letters*, *249*(3), pp.133-147.

Carporzen, L., Weiss, B.P., Elkins-Tanton, L.T., Shuster, D.L., Ebel, D., Gattacceca, J., 2011, Magnetic evidence for a partially differentiated carbonaceous chondrite parent body, Proceedings of the National Academy of Sciences, vol. 108, pp.6386-6389.

Coe, R.S. and Kirby, S.H., 1975. The orthoenstatite to clinoenstatite transformation by shearing and reversion by annealing: mechanism and potential applications. *Contributions to Mineralogy and Petrology*, *52*(1), pp.29-55.

Connelly, J.N., Amelin, Y., Krot, A.N. and Bizzarro, M., 2008. Chronology of the solar system's oldest solids. *The Astrophysical Journal Letters*, *675*(2), p.L121.

Desch, S.J., Morris, M.A., Connolly, H.C., Boss, A.P., 2012, The importance of experiments: Constraints on chondrule forming models, Meteoritics & Planetary Science, vol. 47, pp.1139-1156.

Dodd, R.T., Van Schmus, W.R. and Koffman, D.M., 1967. A survey of the unequilibrated ordinary chondrites. *Geochimica et Cosmochimica Acta*, *31*(6), pp.921-951.

Doyle, P.M., Jogo, K., Nagashima, K., Krot, A.N., Wakita, S., Ciesla, F.J., Hutcheon, I.D., 2015, Early aqueous activity on the ordinary and carbonaceous chondrite parent bodies recorded by fayalite, nature communications, vol.

Ebel, D.S., Leftwich, K., Brunner, C.E. and Weisberg, M.K., 2009, March. Abundance and size distribution of inclusions in CV3 chondrites by X-ray image analysis. In *Lunar and Planetary Science Conference* (Vol. 40, p. 2065).

Fegley, B. and Palme, H., 1985. Evidence for oxidizing conditions in the solar nebula from Mo and W depletions in refractory inclusions in carbonaceous chondrites. *Earth and Planetary Science Letters*, *72*(4), pp.311-326.
Garenne, A., Beck, P., Montes-Hernandez, G., Chiriac, R., Toche, F., Quirico, E., Bonal, L., Schmitt, B., 2014, The abundance and stability of "water" in type 1 and 2 carbonaceous chondrites (CI, CM and CR), *Geochimica et Cosmochimica Acta*, vol. 137, pp. 93-112.

Fruland, R.M., McKay, D.S. and King, E.A., 1978. Allende dark inclusions. In*Lunar and Planetary Science Conference Proceedings* (Vol. 9, pp. 1305-1329).

Gooding, J.L. and Keil, K., 1981. Relative abundances of chondrule primary textural types in ordinary chondrites and their bearing on conditions of chondrule formation. *Meteoritics*, *16*(1), pp.17-43.

Greeley, R., Lancaster, N., Lee, S. and Thomas, P., 1992. Martian aeolian processes, sediments, and features. *Mars*, *1*, pp.730-766.

Grossman, L., 1972. Condensation in the primitive solar nebula. *Geochimica et Cosmochimica Acta*, *36*(5), pp.597-619.

Hewins, R.H., Connolly, H.C., Lofgren Jr, G.E. and Libourel, G., 2005, December. Experimental constraints on chondrule formation. In *Chondrites and the protoplanetary disk* (Vol. 341, p. 286).

Hezel, D.C., Friedrich, J.M. and Uesugi, M., 2013. Looking inside: 3D structures of meteorites. *Geochimica et Cosmochimica Acta*, (116), pp.1-4.

Hood, L.L., Ciesla, F.J., Artemieva, N.A., Marzari, F. and Weidenschilling, S.J., 2009. Nebular shock waves generated by planetesimals passing through Jovian resonances: Possible sites for chondrule formation.*Meteoritics & Planetary Science Archives*, *44*(3), pp.327-342.

Hua, X., Zinner, E.K. and Buseck, P.R., 1996. Petrography and chemistry of fine-grained dark rims in the Mokoia CV3 chondrite: Evidence for an accretionary origin. *Geochimica et cosmochimica acta*, *60*(21), pp.4265-4274.

Kimura, M. and Ikeda, Y., 1995. Anhydrous alteration of Allende chondrules in the solar nebula II: Alkali-Ca exchange reactions and formation of nepheline, sodalite and Ca-rich phases in chondrules. *Antarctic Meteorite Research*, *8*, p.123.

Kojima, T. and Tomeoka, K., 1996. Indicators of aqueous alteration and thermal metamorphism on the CV parent body: Microtextures of a dark inclusion from Allende. *Geochimica et Cosmochimica Acta*, *60*(14), pp.2651-2666.

Kornacki, A.S., Wood, J.A., 1984, The mineral chemistry and origin of inclusion matrix and meteorite matrix in the Allende CV3 chondrite, *Geochmica et Cosmochimica Acta*, vol. 48, pp.1663-1676.

Kring, D.A. and Cohen, B.A., 2002. Cataclysmic bombardment throughout the inner solar system 3.9–4.0 Ga. *Journal of Geophysical Research: Planets*,*107*(E2).

Krot, A.N., Scott, E.R. and Zolensky, M.E., 1995. Mineralogical and chemical modification of components in CV3 chondrites: Nebular or asteroidal processing?. *Meteoritics*, *30*(6), pp.748-775.

Krot, A.N., Petaev, M.I., Scott, E.R., CHOI, B.G., Zolensky, M.E. and Keil, K., 1998. Progressive alteration in CV3 chondrites: More evidence for asteroidal alteration. *Meteoritics & Planetary Science*, *33*(5), pp.1065-1085.

Krot, A.N., Petaev, M.I. and Bland, P.A., 2004. Multiple formation mechanisms of ferrous olivine in CV carbonaceous chondrites during fluid-assisted metamorphism. *Antarctic meteorite research*, *17*, p.153.

Krot, A.N., Yurimoto, H., Hutcheon, I.D. and MacPherson, G.J., 2005. Chronology of the early Solar System from chondrule-bearing calcium-aluminium-rich inclusions. *Nature*, *434*(7036), pp.998-1001.

Krot, A.N., Amelin, Y., Bland, P., Ciesla, F.J., Connelly, J., Davis, A.M., Huss, G.R., Hutcheon, I.D., Makide, K., Nagashima, K. and Nyquist, L.E., 2009. Origin and chronology of chondritic components: A review. *Geochimica et Cosmochimica Acta*, *73*(17), pp.4963-4997.

Libourel, G., Krot, A.N. and Tissandier, L., 2006. Role of gas-melt interaction during chondrule formation. *Earth and Planetary Science Letters*, *251*(3), pp.232-240.

Lofgren, G. and Russell, W.J., 1986. Dynamic crystallization of chondrule melts of porphyritic and radial pyroxene composition. *Geochimica et Cosmochimica Acta*, *50*(8), pp.1715-1726.

Lofgren, G. and Lanier, A.B., 1990. Dynamic crystallization study of barred olivine chondrules. *Geochimica et Cosmochimica Acta*, *54*(12), pp.3537-3551.

Lorenz, R.D., Lunine, J.I., Grier, J.A. and Fisher, M.A., 1995. Prediction of aeolian features on planets: Application to Titan paleoclimatology. *Journal of Geophysical Research: Planets*, *100*(E12), pp.26377-26386.

Mcsween, H.Y., 1977. Petrographic variations among carbonaceous chondrites of the Vigarano type. *Geochimica et Cosmochimica Acta*, *41*(12), pp.1777-1790.

McSween, H.Y., 1979. Alteration in CM carbonaceous chondrites inferred from modal and chemical variations in matrix. *Geochimica et Cosmochimica Acta*, *43*(11), pp.1761-1770.

Marrocchi, Y. and Libourel, G., 2013. Sulfur and sulfides in chondrules.*Geochimica et Cosmochimica Acta*, *119*, pp.117-136.

Metzler, K., Bischoff, A., Stoeffler, D., 1992, Accretionary dust mantles in CM chondrites: Evidence for solar nebula processes, Geochimica et Cosmochimica Acta, vol. 56, pp.2873-2897.

Nakamoto, T., Hayashi, M.R., Kita, N.T. and Tachibana, S., 2005, December. Chondrule-forming shock waves in the solar nebula by X-ray flares. In*Chondrites and the protoplanetary disk* (Vol. 341, p. 883).

Nemtchinov, I.V., Shuvalov, V.V., Artemieva, N.A., Kosarev, I.B. and Popel, S.I., 2002. Transient atmosphere generated by large meteoroid impacts onto an atmosphereless cosmic body: gasdynamic and physical processes.*International journal of impact engineering*, *27*(5), pp.521-534.

Potter, A.E. and Morgan, T.H., 1998. Coronagraphic observations of the lunar sodium exosphere near the lunar surface. *Journal of Geophysical Research: Planets*, *103*(E4), pp.8581-8586.

Prior, G.T., 1920. The classification of meteorites. *Mineral. Mag*, *19*, pp.51-63.

Prior, D.J., Boyle, A.P., Brenker, F., Cheadle, M.C., Day, A., Lopez, G., Peruzzo, L., Potts, G.J., Reddy, S., Spiess, R. and Timms, N.E., 1999. The application of electron backscatter diffraction and orientation contrast imaging in the SEM to textural problems in rocks. *American Mineralogist*, *84*(11-12), pp.1741-1759.

Putnis, A., 2009. Mineral replacement reactions. *Reviews in mineralogy and geochemistry*, *70*(1), pp.87-124.

Ryan, E.V. and Melosh, H.J., 1998. Impact fragmentation: From the laboratory to asteroids. *Icarus*, *133*(1), pp.1-24.

Scott, E.R. and Taylor, G.J., 1983. Chondrules and other components in C, O, and E chondrites: Similarities in their properties and origins. *Journal of Geophysical Research: Solid Earth*, *88*(S01).

Scott, E.R., Keil, K. and Stöffler, D., 1992. Shock metamorphism of carbonaceous chondrites. *Geochimica et Cosmochimica Acta*, *56*(12), pp.4281-4293.

Scott, E.R., 2007. Chondrites and the protoplanetary disk. *Annu. Rev. Earth Planet. Sci.*, *35*, pp.577-620.
Shu, F.H., Shang, H., Gounelle, M., Glassgold, A.E. and Lee, T., 2001. The origin of chondrules and refractory inclusions in chondritic meteorites. *The Astrophysical Journal*, *548*(2), p.1029.
Smyth, J.R., 1974. Experimental study on the polymorphism of enstatite.*American Mineralogist*, *59*(3-4), pp.345-352.
Stuart, C.A., Piazolo, S. and Daczko, N.R., 2016. Mass transfer in the lower crust: Evidence for incipient melt assisted flow along grain boundaries in the deep arc granulites of Fiordland, New Zealand. *Geochemistry, Geophysics, Geosystems*.
Takayama, A. and Tomeoka, K., 2012. Fine-grained rims surrounding chondrules in the Tagish Lake carbonaceous chondrite: Verification of their formation through parent-body processes. *Geochimica et Cosmochimica Acta*, *98*, pp.1-18.
Spruzeniece, L., Piazolo, S., Maynard-Casely, H.E., 2016. Deformation-resembling microstructure created by fluid-mediated dissolution-precipitation reactions. Manuscript Submitted.
Strobl, M., Manke, I., Kardjilov, N., Hilger, A., Dawson, M. and Banhart, J., 2009. Advances in neutron radiography and tomography. *Journal of Physics D: Applied Physics*, *42*(24), p.243001.
Tissandeer, L., Libourel, G. and Robert, F., 2002. Gas-melt interactions and their bearing on chondrule formation. *Meteoritics & Planetary Science*,*37*(10), pp.1377-1389.
Tomeoka, K. and Ohnishi, I., 2015. Redistribution of chondrules in a carbonaceous chondrite parent body: A model. *Geochimica et Cosmochimica Acta*, *164*, pp.543-555.
Turner, F.J., Heard, H. and Griggs, D.T., 1960. Experimental deformation of enstatite and accompanying inversion to clinoenstatite. In *Report of 21st International Geological Congress, Copenhagen* (Vol. 18, pp. 399-408).
Wasson, J.T. and Kallemeyn, G.W., 1988. Compositions of chondrites.*Philosophical Transactions of the Royal Society of London A: Mathematical, Physical and Engineering Sciences*, *325*(1587), pp.535-544.
Watt, L.E., Bland, P.A., Prior, D.J., Russell, S.S., 2006, Fabric analysis of Allende matrix using EBSD, *Meteoritics & Planetary Science*, vol. 41, pp.989-1001.
Weisberg, M. K., McCoy, T. J., & Krot, A. N., 2006), Systematics and evaluation of meteorite classification. *Meteorites and the early solar system II*, *19*.
Wheeler, J., Prior, D., Jiang, Z., Spiess, R. and Trimby, P., 2001. The petrological significance of misorientations between grains. *Contributions to Mineralogy and Petrology*, *141*(1), pp.109-124.
Wlotzka, F., 1993. A weathering scale for the ordinary chondrites.*Meteoritics*, *28*, pp.460-460.
Wood, J.A., 1963. On the origin of chondrules and chondrites. *Icarus*, *2*, pp.152-180.
Wood, J.A., 1988. Chondritic meteorites and the solar nebula. *Annual Review of Earth and Planetary Sciences*, *16*, pp.53-72.
Yin, Q., Jacobsen, S.B., Yamashita, K., Blichert-Toft, J., Télouk, P. and Albarede, F., 2002. A short timescale for terrestrial planet formation from Hf–W chronometry of meteorites. *Nature*, *418*(6901), pp.949-952.
Young, E.D., Zhang, K.K. and Schubert, G., 2003. Conditions for pore water convection within carbonaceous chondrite parent bodies–Implications for planetesimal size and heat production. *Earth and Planetary Science Letters*,*213*(3), pp.249-259.
Zolensky, M., Barrett, R. and Browning, L., 1993. Mineralogy and composition of matrix and chondrule rims in carbonaceous chondrites. *Geochimica et Cosmochimica Acta*, *57*(13), pp.3123-3148.
Zolensky, M. and McSween Jr, H.Y., 1988. Aqueous alteration. *Meteorites and the early solar system*, *1*, pp.114-143.
Zolotov, M.Y., Mironenko, M.V. and Shock, E.L., 2006. Thermodynamic constraints on fayalite formation on parent bodies of chondrites. *Meteoritics & Planetary Science*, *41*(11), pp.1775-1796.

Supplementary

Chapter 1

Table 1.1 Properties of chondrite groups. Adapted from Scott & Krot (2003).

Group	Type	Refractory inclusions (vol.%)	Chondrule (vol.%)	Chondrule ave. diameter (mm)	Fe,Ni metal (vol.%)	Matrix (vol.%)	Examples
Carbonaceous							
CI	1	<0.01	<5	-	<0.1	95	Ivuna, Orguiel
CM	1-2	5	20	0.30	0.1	70	Murchison
CO	3	13	40	0.15	1-5	30	Ornans
CV	2-3	10	45	1	0-5	40	Vigarano, Allende
CK	3-6	4	15	0.8	<0.1	75	Karoonda
CR	1-2	0.5	50-60	0.7	3-8	30-50	Renazzo
CH	3	0.1	70	0.05	20	5	ALH 85085
CB_a	3	<0.1	46	5	60	<5	Bencubbin
CB_b	3	<0.1	30	0.5	70	<5	QUE 94411
Ordinary							
H	3-6	<0.1	60-80	0.3	8	10-15	Dhajala
L	3-6	<0.1	60-80	0.5	3	10-15	Khohar
LL	3-6	<0.1	60-80	0.6	1.5	10-15	Semarkona
Enstatite							
EH	3-6	<0.1	60-80	0.2	8	<0.1-10	Qingzhen, Abee
EL	3-6	<0.1	60-80	0.6	1.5	<0.1-10	Hvittis
Other							
K	3	<0.1	20-30	0.6	6-9	70	Kakangari
R	3-6	<0.1	>40	0.4	<0.1	35	Rumuruti

Chapter 2

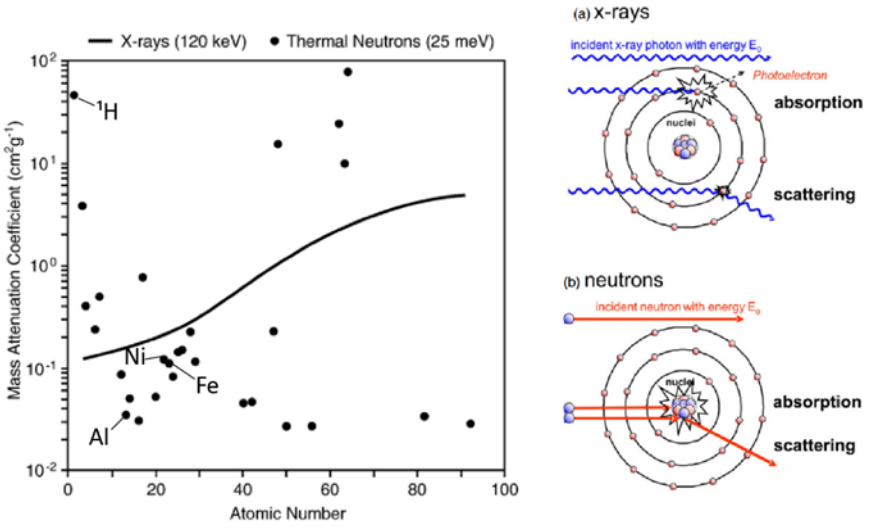

Figure 2.1 Left: Thermal neutron (25 MeV) and x-ray (100 KeV) mass attenuation coefficients based on atomic number. Right: Interaction of x-rays with the electron shell (a) results in a near monotonic increase in the attenuation coefficient. Nuclear Interaction of neutrons (b) with different elements doesn't increase regularly with atomic number, different isotopes of the same element can have significantly different attenuation coefficients. Modified after Strobl et al. (2009).

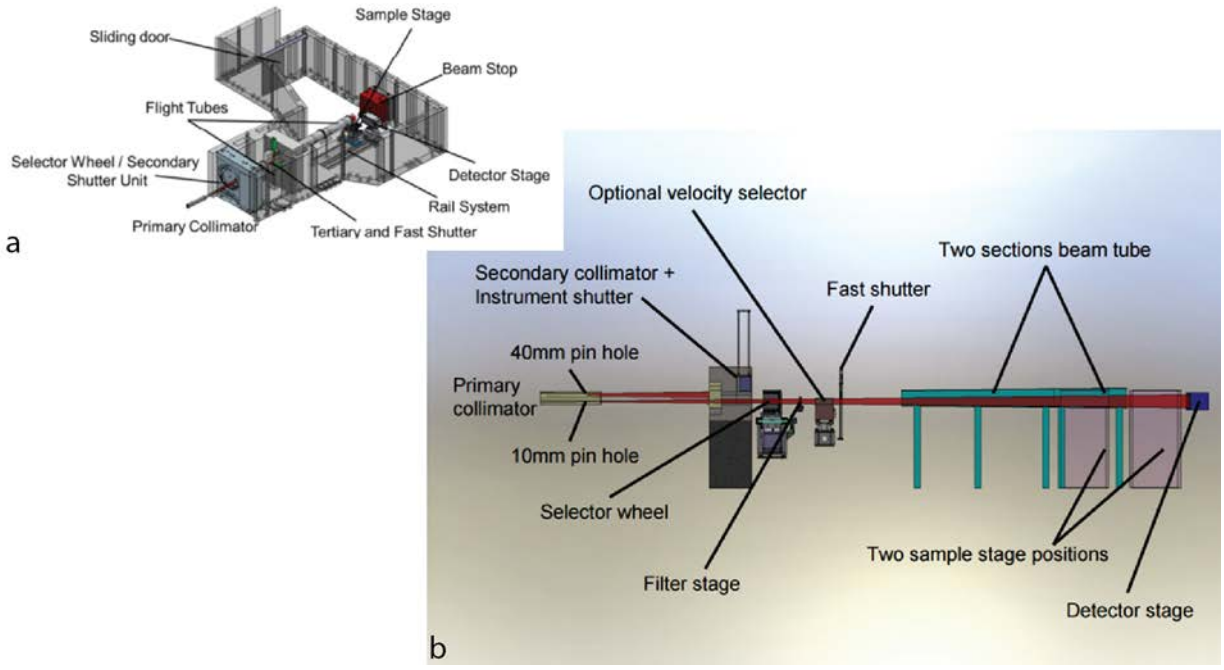

Figure 2.2 Schematic diagram of the DINGO neutron imaging instrument (a) and beam path with high resolution setting (b). Modified after Garbe et al. (2011).

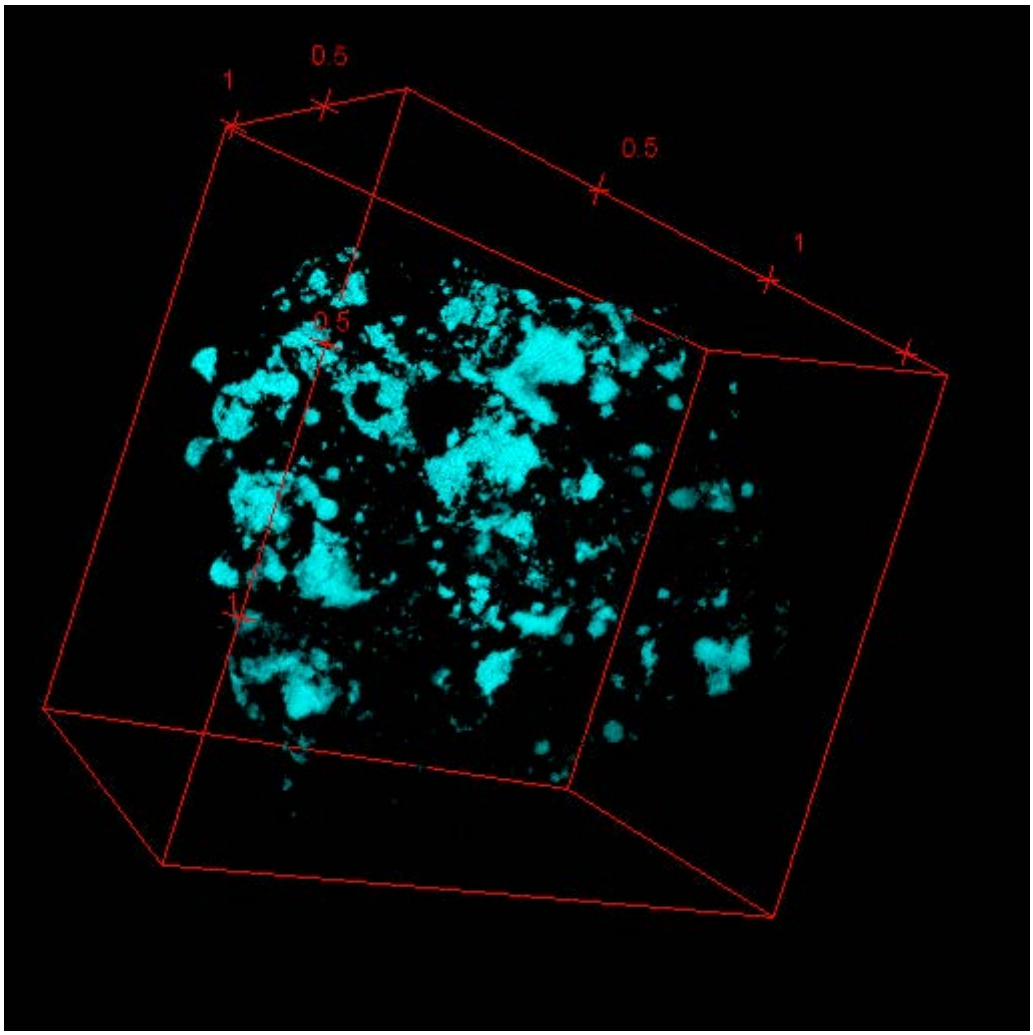

Fig. 2.3 Distribution of fayalite rich alteration in the NWA3118 chondrite

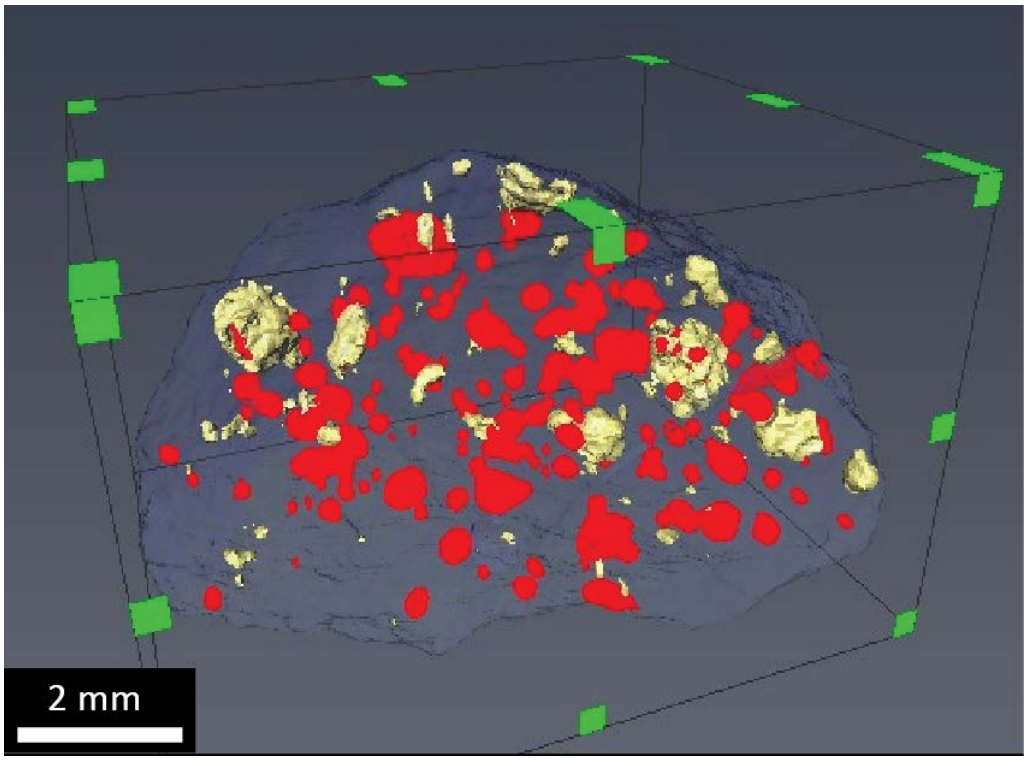

Fig. 2.4 3D volume render of Murchison with transparent matrix showing the distribution of chondrules (red) and areas of high attenuation (yellow). Areas of high attenuation are found surrounding chondrules and as discrete fragments in the matrix.

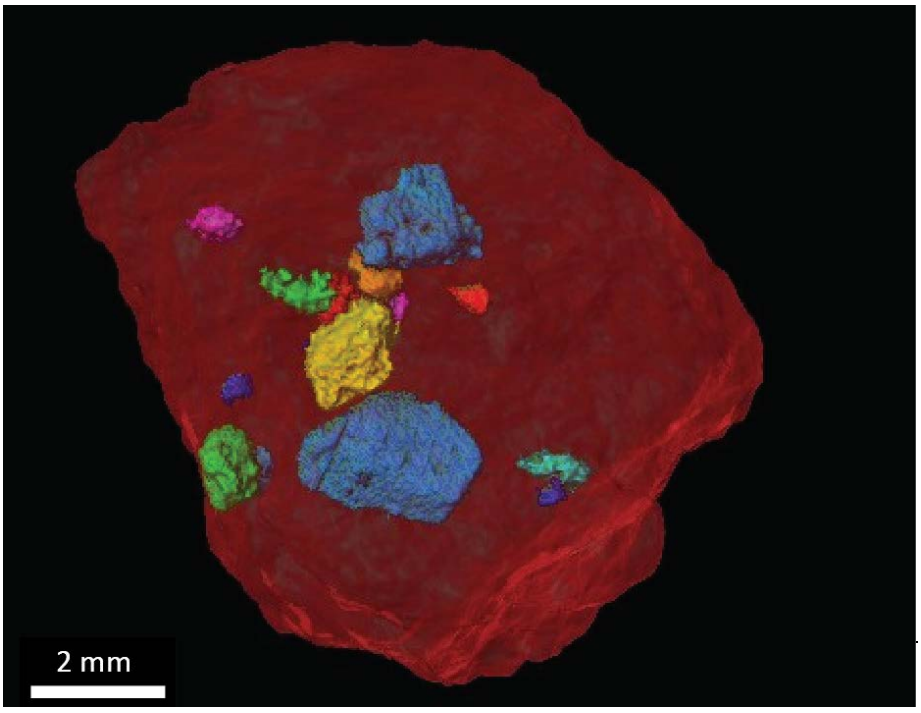

Fig. 2.5 3D volume render of Nagoya with transparent matrix showing the shape, size and distribution of hydrated clasts.

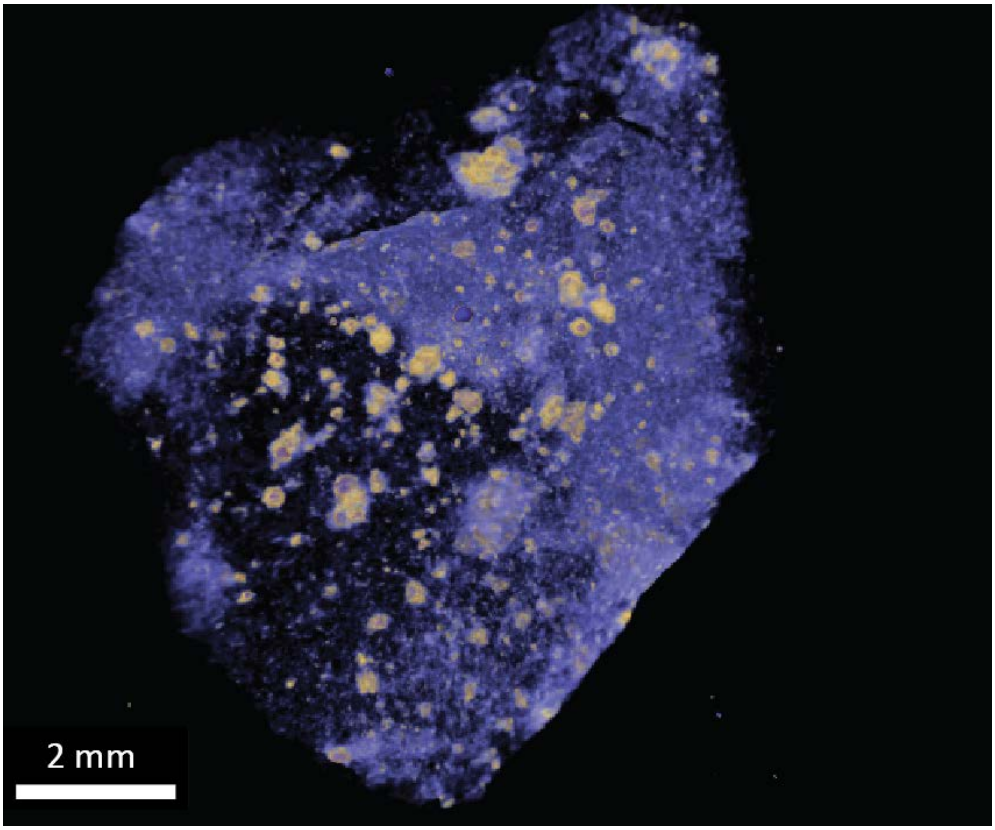

Fig. 2.6 3D volume render of Sutter's Mill with no matrix. CM lithologies appear as small spherical clasts (yellow). The hydration band can be seen to wrap around the sample (light blue).

Chapter 3

Table 3.1 Textural and composition classification for chondrules presented by Gooding & Keil (1981) and McSween (1977). Modified after Lauretta et al. (2006).

Textural Classification			
Abbreviation	Texture		
POP	Porphyritic, both olivine and pyroxene		
PO	Porphyritic, dominated by olivine (>10/1 by volume)		
PP	Porphyritic, dominated by pyroxene (>10/1 by volume)		
RP	Radial pyroxene		
BO	Barred olivine		
CC	Cryptocrystalline		
GOP	Granular olivine-pyroxene		
M	Metallic		
Compositional Classification			
Type	Silicate composition	Subtype	Silicate abundances
I	FeO-poor (Fo, En > 90)	A	Abundant olivine (>80 vol%)
		AB	Intermediate abundances of olivine and pyroxene
II	FeO-rich (Fo, En < 90)	B	Abundant pyroxene (>80 vol%)

Chondrule	Group	Type	Sub-type
All-001	2	A	1.2
All-002	1	AB	1.4
All-003	2	AB	1.5
All-004	2	A	1.4
All-005	2	A	1.4
All-006	2	AB	1.2
All-007	2	AB	1.4
All-008	2	A	1.3
All-009	2	A	1.4
All-010	2	A	1.4
All-011	2	AB	1.4
All-012	2	B	1.2
All-013	2	A	1.4
All-014	2	A	1.6
All-015	1	A	1.4
All-016	2	A	1.3
All-017	2	B	1.4
NWA3-001	2	A	1.7
NWA3-002	2	B	1.8
NWA3-003	2	A	1.7
NWA3-004	2	A	1.7
NWA3-005	2	A	1.7
NWA3-006	1	AB	1.6
NWA3-007	1	A	1.7
NWA3-008	2	B	1.9
NWA3-009	2	A	1.7
NWA3-010	2	AB	1.8
NWA3-011	2	AB	1.7
NWA3-012	2	B	1.7
NWA3-013	2	A	1.6
NWA3-014	2	A	1.5
NWA4-001	2	A	1.3
NWA4-002	2	A	1.2
NWA4-003	2	AB	1.3
NWA4-004	2	A	1.3
NWA4-005	2	AB	1.3
NWA4-006	2	A	1.1
NWA4-007	2	A	1.1
NWA4-008	2	A	1.1
NWA4-009	2	A	1
NWA4-010	2	B	1.2
NWA4-011	2	A	1.1
NWA4-012	2	AB	1.3
NWA4-013	2	B	1.5
NWA4-014	2	B	1.2
NWA4-015	1	A	1.2
NWA4-016	1	A	1.1
NWA4-017	2	B	1.2

Table 3.2 Classification of chondrules surveyed from Allende, NWA3118 and NWA4502.